https://doi.org/10.5194/egusphere-2023-2636
Preprint. Discussion started: 15 November 2023

Particle size distributions in Earth Sciences: a review of techniques and a new procedure to match 2D and 3D analyses

Mattia Pizzati[1]*, Luciana Mantovani[1], Antonio Lisotti[2], Fabrizio Storti[1] and Fabrizio Balsamo[1]

[1]*University of Parma, Department of Chemistry, Life Sciences, and Environmental Sustainability, 43124 Parma, Italy.*

[2]*University of Parma, Information Management Area, 43124 Parma, Italy.*

* *Corresponding author, E-mail address: mattia.pizzati@unipr.it, phone number: +39 0521905202*

ABSTRACT

Particle size is an essential tool in many research areas spanning from Earth Sciences, Engineering, Material Sciences, Soil Sciences and Pharmacology, among others. Over the last decades, several techniques and methodologies have been developed to calculate particle size distributions on different sample types (i.e., cohesive versus loose), spanning from volumetric (3D) to image-aided (2D) analyses. Here, we (1) present a critical review of most commonly used techniques to calculate particle size distributions from cohesive and loose samples, and (2) we illustrate a new calculation formula to extract reliable 3D grain size distributions from 2D datasets. We propose the use of the "corrected volume-weighted mean diameter" (D_w), as a new particle size descriptor, which results from the summation of products between equivalent particle diameter and particle volume, divided by the total volume of analyzed particles. In this calculation, particles were approximated to perfect circles-spheres, but a shape correction factor was applied to consider deviations from the perfect spherical shape. We tested the accuracy of D_w calculation formula by analyzing 2D datasets acquired from thin sections of 5 selected granular sand samples having different mean grain diameters and grain size distributions (i.e., different sorting degree, grain size distribution width and skewness). Grains were manually digitized, and per each thin section more than 5,000 particles were acquired. Two-dimensional grain size distributions were cross-checked with the results provided via laser diffraction granulometry on the same samples and were compared with previously published and widely used calculation methods. Our promising results encourage the usage of D_w formula as it provides best matching results with 3D laser granulometry and needs basic input parameters that can be easily extracted from any image analysis software.

Keywords

Particle size distribution; equivalent diameter; volume-weighted mean diameter; granular materials; image analysis technique; laser diffraction granulometry.

1. Introduction

1.1 Particle size analysis in Earth Sciences and beyond

The quantification of particle size distribution is a fundamental parameter to be determined in different scientific disciplines spanning from Earth and Planetary Sciences, Engineering, Life Sciences, Material Sciences, Soil Sciences, and Pharmacology. Particle size is defined as a scalar property of granular media and is typically calculated as the nominal diameter of particles (Udden, 1914; Wentworth, 1922; Krumbein and Pettijohn, 1938; Krumbein and Sloss, 1963; Pettijohn et al., 1972). Particle size is a fundamental component of the texture of granular materials (sediments, rocks, and aggregates) together with particle shape (Wadell, 1935; Krumbein, 1941a; Moss, 1962; Krumbein and Sloss, 1963; Barrett, 1980; Mora and Kwan, 2000), rounding degree (Wadell, 1933; Powers, 1953; Taylor, 2002),

https://doi.org/10.5194/egusphere-2023-2636
Preprint. Discussion started: 15 November 2023

surface morphological features (Wentworth, 1919; Bowman et al., 2001; Russ, 1990), overall fabric (particle preferred orientation) (Griffiths, 1961), and mineralogical composition (Krumbein and Sloss, 1963; Folk, 1974; Boggs, 2009). In particular, in the field of Earth Sciences, particle size determination plays a major role in stratigraphic and sedimentological studies where it provides fundamental information related to the physical and dynamic transport processes (Krumbein, 1941b; Spencer, 1952; Folk and Ward, 1957; Bull, 1962; Sahu, 1964; Middleton, 1976; Goldbery and Richardson, 1989; Kranck, 1984; Pickering and Hiscott, 2015), provenance and maturity of clastic sediments and rocks (Dapples et al., 1953; Cadigan, 1961; Folk, 1974; Boggs, 2009; Garzanti, 2019), fluid storage potential of sedimentary sequences (Fraser, 1935; Griffiths, 1952) and recognition of sedimentary environments (Keller, 1945; Buller and McManus, 1973; Mutti, 1992; Selley, 2001; Nichols, 2009). Particle size quantification is also fundamental in structural geology studies, where the correct definition of clast-grain size provides important information to constrain brittle deformation mechanisms from fault rock analysis (Blenkinsop, 1991; Storti et al., 2003; Billi, 2005; Heilbronner and Keulen, 2006; Keulen et al., 2007; Luther et al., 2013; Montheil et al., 2020), to understand the overall faulting processes (Engelder, 1974; Sibson, 1977; Marone and Scholz, 1989; Doan and Gary, 2009; Sammis and Ben-Zion, 2008; Balsamo and Storti, 2011), and to define plastic deformation styles (Ranalli, 1984; Freeman and Ferguson, 1986; Stipp and Tullis, 2003; Passchier and Trouw, 2005; Hirsch, 2008; Lopez-Sanchez and Llana-Fúnez, 2016). Planetary geology employs the analysis of particle size to unravel sedimentary and surficial transport processes on terrestrial planets of the Solar System (De Pater and Lissauer, 2001; Faure and Mensing, 2007; Bridges and Muhs, 2012; Grotzinger and Milliken, 2012), and to study meteoritic bodies (Dodd, 1976; Hughes, 1978a; Martin and Mills, 1978; Eisenhour, 1996). Petrophysics takes into account the evaluation of particle size to understand the primary and secondary porosity and overall fluid flow patterns and magnitude through porous media (Tiab and Donaldson, 2004; Torabi and Fossen, 2009;

https://doi.org/10.5194/egusphere-2023-2636
Preprint. Discussion started: 15 November 2023

Balsamo et al., 2010). Hydrogeology studies deal with the quantification of grain size to document fluid pathways in deformed and undeformed rocks and soils (Davis and DeWiest, 1966; Fetter, 1994; Bense et al., 2013). Particle size determination is also important in the field of diagenesis, as in the case of ore-mineral deposits in conjunction with studies regarding structural geology (Jébrak, 1997) or selective cementation of sedimentary sequences (McBride et al., 1995; Mozley and Davis, 1996; Morad et al., 2000; Dutton et al., 2002; Cavazza et al., 2009; Van Den Bril and Swennen, 2009; Balsamo et al., 2012; Pizzati et al., 2018; Dimmen et al., 2020). Geomorphology employs particle size analysis to identify the products of various geomorphic agents in different environments (marine, fluvial and continental) (Easterbrook, 1969). Glaciology extensively implements particle size determination to quantitatively describe the past and present glacial-related deposits (different types of moraines, tills, and cryo-clastic materials) and to define glacier evolution over time (Washburn, 1979; Molnia, 1983; Eicken, 1993; Menzies, 2000). Particle-crystal size is adopted also in petrology of both intrusive and effusive igneous rocks, where it can provide constraints regarding crystal growth processes occurring inside magma chambers (Higgins, 1994; Means and Park, 1994; Bryon et al., 1995; Higgins, 2000; Zieg and Marsh, 2002; Mock and Jerram, 2005; Gualda, 2006; Morgan and Jerram, 2006; Jerram and Higgins, 2007; Jerram et al., 2009). Volcanology is particularly interested in particle size analysis to define the magnitude of past eruptions (Kaminski and Jaupart, 1998), to infer the explosivity index (Giachetti et al., 2021) and to characterize the texture and sedimentary transport mechanisms of volcaniclastic deposits (McPhie et al., 1993; Eychenne and Engwell, 2022).

The broad list of fields of application reported above helps to understand the critical importance of particle size determination as an effective tool to constrain a wide variety of physical processes. The techniques employed to calculate particle size distribution span

https://doi.org/10.5194/egusphere-2023-2636
Preprint. Discussion started: 15 November 2023

from three-dimensional volumetric analysis performed on bulk materials (e.g., classical sieve analysis applied to loose samples) (Udden, 1914) up to bi-dimensional automated-manual image analysis (e.g., using thin section images of cohesive samples) (Heilbronner and Barrett, 2014). Nowadays, laser diffraction-based techniques provide accurate, precise, and relatively fast 3D particle size determination and is particularly effective in the case of loose powder samples (Agrawal et al., 1991). In the field of Earth Sciences, rock samples may show different degrees of cohesion, thus implying the use of different techniques in defining grain size distributions. Unfortunately, the direct comparison among results from different analytical procedures is not straightforward, thus limiting the ability of researchers to compare data obtained in different times and from different case studies. This limitation is even more important when results from 3D and 2D analyses need to be compared. The reason for such discrepancy between 3D and 2D analyses lies in the type of samples (Cortinovis et al., 2019), number of analyzed particles (Lopez-Sanchez, 2020), particle shape and density (Matthews, 1991a), and instrumental limitations associated with the resolution in the upper and lower grain size ranges (Syvitski et al., 1991a).

In the present contribution, we first provide a critical review of available 3D and 2D analytical techniques employed for grain size calculation and related correction methods. Techniques are critically revised highlighting pros, cons, weaknesses, strengths, and applicability on different sample types. Then we focus on defining and testing a new conversion equation to extract 3D average grain diameters from 2D granulometric distributions. To this end, we calculated 2D grain size distributions of 5 selected sand samples through image analysis technique from petrographic thin sections. The obtained results were corrected with literature methods and with our new equation and were compared with data gained by 3D laser diffraction granulometry technique, which served as reference benchmark. A shape correction factor was applied to the calculated mean diameter to consider particle deviations

https://doi.org/10.5194/egusphere-2023-2636
Preprint. Discussion started: 15 November 2023

from the perfect circular shape. In our case, the correction factor was grounded to particle shape, and it slightly varied according to the sample to be analyzed. The volume-weighted mean diameter (D_w) equation provided well matching results with optical granulometry data and proved to be a reliable and an easy-to-use tool to analyze samples with different particle size distributions, textures, sorting degrees, and mineralogical compositions.

1.2 Particle size distribution analysis techniques: a review

Since the beginning of the last century, particle size was measured adopting the metric dimensional scale (Wentworth, 1922), which then became the standard sedimentological scale and it is still widely adopted nowadays (Fig. 1). However, in the following years, a base-2 logarithm scale, also known as the phi-scale (Φ), was proposed (Krumbein, 1938; Krumbein and Sloss, 1963). Due to the diversity of objects to be characterized, particle size has historically been achieved through the adoption of several methods. The first and simplest employed technique was the direct analysis of particles in the field by caliper or tape measurements (Wentworth, 1922). This methodology was mainly used in the case of coarse-grained materials (coarse gravels, pebbles, cobbles, and boulders), for which size determination was easier, but could not be applied with the same precision to fine-grained media. Sieve analysis has been, and it still is, largely adopted to quickly define the particle size of loose granular media and works well in the case of coarse to medium-grained samples (Udden, 1914; Rosenfeld et al., 1953; Friedman, 1962a; Van Der Plas, 1962; Krumbein and Sloss, 1963; Folk, 1966). However, this method struggles in properly characterizing the size of fine-grained fractions (< 31-62.5 µm), which must be analyzed with other, specifically designed, techniques (Krumbein, 1932; Singer et al., 1988; Bianchi et al., 1999) (Fig. 1).

https://doi.org/10.5194/egusphere-2023-2636
Preprint. Discussion started: 15 November 2023

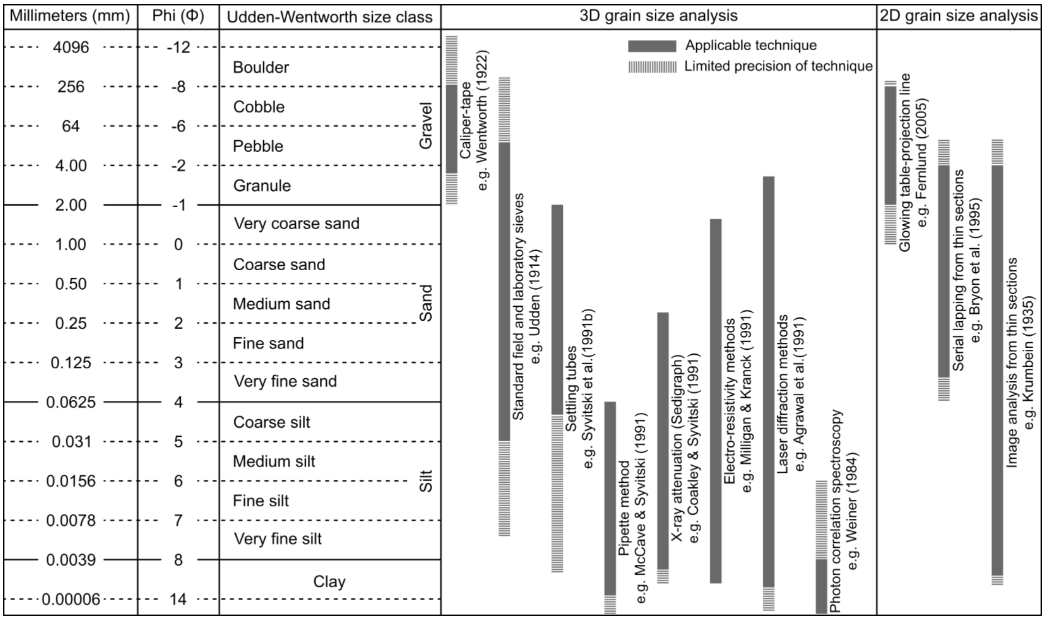

Figure 1. Most common techniques applied in grain size analysis with analytical upper and lower size boundaries. For a comprehensive literature background of the reported methodologies the reader is referred to the introduction section 1.2.

The adoption of electro-formed sieves may extend the granulometric range down to the fine silt size (> 5 µm), however this procedure is impractical and requires specifically designed sieves. Sieving allows the definition of the intermediate axis of particles, considering particles as anisotropic ellipses, defined by a major (a), intermediate (b) and a minor (c) axis, and can be used to build mass or volume distribution curves (Bush, 1951; Adams, 1977). Sieving is typically coupled with sedimentation and pipette analysis to cover the finest (clay and silt-size particles) fractions of granular samples (Syvitski et al., 1991a; Krumbein and Pettijohn, 1938; McCave and Syvitski, 1991). However, these techniques may show pitfalls in matching sieving and sedimentation-pipette results in one single granulometric curve and are also time-consuming and not suitable to analyze large sample amounts (Syvitski et al., 1991b; Beuselinck et al., 1998; Bittelli et al., 2019) (Fig. 1). For coarse-grained granular samples (sizes > 2 mm), image analysis technique applied to particles or grains manually

https://doi.org/10.5194/egusphere-2023-2636
Preprint. Discussion started: 15 November 2023

dispersed on a glowing table was adopted and the projection of the particle boundaries was used to reconstruct their volume and size (Fernlund, 2005). Such a technique proved to be useful in the case of relatively coarse and well disaggregated samples, while it showed limitations dealing with fine-grained or aggregate particles (Fig. 1). The detailed analysis of particle images was implemented also in digital sieving software, coupled with statistical programs (Matlab®), particularly useful to determine the size of loose medium to coarse-grained materials (Kwan et al., 1999; Tafesse et al., 2012). Again, the limitations of this methodology reside in the scarcely representative number of analyzed particles and in the relatively tiny grain size span that can be considered (Fig. 1). In the last decades, the introduction of light diffraction instruments allowed to automatically analyze samples with wide grain size ranges (from clay to gravel) in a single analytical process (de Boer et al., 1987; Agrawal et al., 1991; Blott et al., 2004; Sperazza et al., 2004; Bah et al., 2009). Optical granulometry provides reliable and relatively quick analyses, resulting particularly indicated in the case of numerous samples (Kimura et al., 2018; Brooks et al., 2022). However, reliability of results may depend upon the chosen instrumental parameters, which should be carefully tested to minimize sample alteration (Matthews, 1991; Konert and Vandenberghe, 1997; Blott and Pye, 2006; Storti and Balsamo, 2010; Schulte et al., 2016; Celia Magno et al., 2018; Cortinovis et al., 2019). Moreover, sample treatment, either chemical or mechanical, before the analysis must be conducted carefully to avoid incorrect or biased results (Folk, 1974; McCave et al., 1986; Matthews, 1991; Maithel et al., 2019). Laser-diffraction-based instruments tend to underestimate the clay fraction especially in the case of particles with equivalent diameter finer than 0.1 µm (Sperazza et al., 2004; Brooks et al., 2022). This issue is mainly related to the dispersion medium, and techniques adopted by most of the available equipment, that are not designed to efficiently disaggregate clay-dominated samples in their constitutive elementary particles (Fig. 1). Techniques relying on electro-resistivity methods, such as the widely used Coulter Counter, measure particle volume based on variations of electrical field induced by grains of different size dispersed in an electrolyte dispersant, which are recorded as electrical pulses with different intensities (Milligan and Kranck, 1991; Beuselinck et al., 1998; Roberson and Weltje, 2014). In a similar way to laser granulometers, electro-resistivity-based instruments have wide applicability in term of particle size but struggle in the clay range (< 2 μm) (Fig. 1). X-ray particle attenuation technique (Sedigraph) uses the attenuation of incident radiation caused by sample suspended in a dispersion medium to calculate the concentration of particles settling from suspension (Coakley and Syvitski, 1991; Bianchi et al., 1999; Celia Magno et al., 2018). This method is accurate in analyzing particles with equivalent diameter from 1 to ~300 μm, while it provides less reliable results outside this grain size interval (McCave and Syvitski, 1991; Cheetham et al., 2008) (Fig. 1). Photon correlation spectroscopy uses the fluctuations of light diffraction generated by Brownian motion of particles suspended in liquid media (Weiner, 1984). This technique is capable of efficiently define the size of particles with equivalent diameter down to 1 nm, thus including colloids and is particularly reliable in the clay size range (Fig. 1).

The techniques described above are particularly indicated for loose or weakly cemented granular samples that can be easily disaggregated in the elementary constitutive particles. Among the methods involved in particle size analysis in the case of indurated or tightly cemented samples that cannot be easily disaggregated, thin sectioning coupled with petrographic analysis has been the most widely used for decades (Krumbein, 1935; Greenman, 1951; Packham, 1955; Friedman, 1958; Basumallick, 1964; Smith, 1966; Kellerhals et al., 1975; Schäfer and Teyssen, 1987; Kennedy and Mazzullo, 1991; Francus, 1999; van den Berg et al., 2003) (Fig. 1). Within the thin section area particles accounted for the analysis may be chosen through the grid point count technique (Chayes, 1949; Friedman, 1965; Folk, 1966), the intersection line (Van Der Plas, 1962; Stauffer, 1966) or via manual-automatic identification (Grassy, 1943; Mazzullo and Kennedy, 1985; Kennedy and Mazzullo, 1991; Heilbronner, 2000; Ketcham, 2005; Heilbronner and Barrett, 2014). This latter procedure may be aided by image analysis software (Seelos and Sirocko, 2005; Schneider et al., 2012; Heilbronner and Barrett, 2014; Liu et al., 2021; Théodon et al., 2023). Image analysis techniques can grant good results in a wide span of particle sizes, from few mm down to the clay fraction (~1 µm), provided that images allow a precise discrimination of fine particles. To this end, image analysis can be performed at several scales of observation spanning from optical microscopy, scanning electron microscopy (SEM) or with transmission electron microscopy (TEM) according to the size of the object to be characterized (Fig. 1). Following thin section cutting, the grain size is determined as the apparent diameter of randomly sectioned particles, which is generally lower than the real or maximum equivalent diameter, a phenomenon known as the corpuscle effect (Wicksell, 1925; Rosenfeld et al., 1953; Burger and Skala, 1976; Boggs, 2009; Lopez-Sanchez and Llana-Fúnez, 2016). In order to gain the real and maximum diameter, particles need to be cut along the equatorial diameter, a peculiar configuration that is rather uncommon in sectioned materials (Krumbein and Sloss, 1963). To avoid discrepancy between granulometric data gained from thin section analysis and other methodologies, several correction factors and equations have been developed. Some of them rely on statistical (Chayes, 1950; Burger and Skala, 1976; Kong et al., 2005), stereological (Elias, 1967; Russ, 1986; Sahagian and Proussevitch, 1998; Gallagher et al., 2023), or theoretical-mathematical treatise (Krumbein, 1935; Sahu, 1966; Cruz-Orive, 1983), considering particles as perfect spheres randomly cut along the thin section plane. Other correction methodologies apply statistical autocorrelation functions (Panozzo Heilbronner, 1992), software-aided projections of digitized particle outlines (Panozzo Heilbronner, 1983) or empirical correction equations (Harrell and Eriksson, 1979) to compare results from image analysis with data acquired by sieving. Some authors attempted to determine the real grain size distributions by sample

https://doi.org/10.5194/egusphere-2023-2636
Preprint. Discussion started: 15 November 2023

serial sectioning to reconstruct the 3D shapes of particles (Bryon et al., 1995; Cooper and Hunter, 1995). Nowadays, there is no univocal correlation function linking particle size data from 2D image analysis to the corresponding 3D grain size distributions acquired either by sieving or light diffraction techniques, because all available conversion tools are sample or method sensitive. This does not allow a direct comparison between grain size data gained by different analytical techniques.

1.3 A new parameter to match 2D and 3D particle size analyses: volume-weighted mean diameter (D_w)

The employed volume-weighted mean diameter (D_w) includes both the equivalent diameter and the shape of analyzed grains. We performed the calculation of volume-weighted mean diameter based on the entire grain size datasets that were extracted from each thin section. The adopted formula operates a weighing of particle diameters according to the volume of the equivalent spheres. Following this, a fine-grained particle influences the final average diameter less than a coarse-grained one. The formula employed for the calculations is:

$$D_w = \left(\frac{\sum_{i=0}^{i=n} d_i * V_i}{\sum_{i=0}^{i=n} V_i} \right) \quad (1)$$

where d_i is the equivalent diameter of the circle having the same area of the traced grains, V_i is the converted spherical volume of grains and i is the number of grains used in the calculation. By developing the formula of spherical volume, equation 1 can be simplified as follows:

$$D_w = \left(\frac{\sum_{i=0}^{i=n} \frac{\pi}{6} * d_i^4}{\sum_{i=0}^{i=n} \frac{\pi}{6} * d_i^3} \right) \quad (2)$$

https://doi.org/10.5194/egusphere-2023-2636
Preprint. Discussion started: 15 November 2023

Grain shape was also implemented in the final calculation of the proposed weighted mean diameter. In particular, we considered the deviation of grains from the perfect two-dimensional circular shape. To this aim, we adopted the λ shape correction factor (surface area correction), which can be calculated from the raw grain size datasets extracted via image analysis as follows (Johnson et al., 2021):

$$\lambda = K * \left(\frac{p_{grain}}{p_{circle}}\right) \tag{3}$$

where p_{grain} is the outer perimeter of the manually traced grain boundary and p_{circle} is the circumference of the equivalent circle having the same area of the grain. *K* is a constant value multiplying the perimeter ratio and can be simplified to 1 in the case of grains with aspect ratio (elongation of particles) comprised between 1 and 10 (Davies et al., 2019; Song et al., 2020). In calculation of λ shape correction factor we used the average values of grain perimeter and equivalent circle circumference to be inserted in equation 3, considering the entire grain size dataset for each thin section. Following this, we implemented the average λ correction factor in equation 2 to develop the corrected volume-weighted mean diameter formula as indicated below:

$$D_w = \lambda * \left(\frac{\sum_{i=0}^{i=n} \frac{\pi}{6} * d_i^4}{\sum_{i=0}^{i=n} \frac{\pi}{6} * d_i^3}\right) \tag{4}$$

4. Analytical methods

4.1 Sampled test sandy sediments

We collected 5 different granular sand samples that were used as benchmarks for comparative grain size determinations through thin sections and optical laser granulometer. All samples were characterized by low to no cohesion and were easily collected by hand or

https://doi.org/10.5194/egusphere-2023-2636
Preprint. Discussion started: 15 November 2023

with sampling tools. About 500 g of sandy materials were collected. Sand specimens belonged to different sedimentological environments spanning from continental-fluvial (braided stream rivers) to shallow marine (beach and deltaic settings) (Fig. 2a).

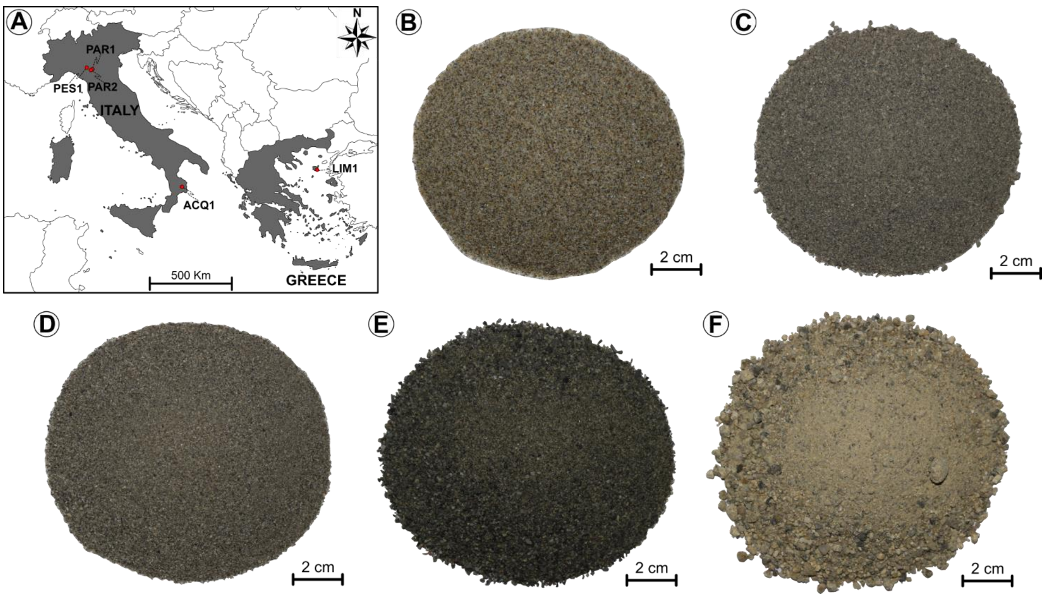

Figure 2. Geographical position and pictures of collected sand samples. (**a**) Central and Eastern Mediterranean Sea area showing the position of collected samples. (**b**) Sample amount LIM1 beach sand from Lemnos Island, NE Greece. (**c**) Sample amount PAR1 from the bottom of a fluvial sand bar collected in the Parma Creek, Northern Apennines. (**d**) Sample amount PAR2 from the top of a fluvial sand bar collected in the Parma Creek, Northern Apennines. (**e**) Sample amount PES1 fluvial sand from the Pessola Creek, Northern Apennines. (**f**) Sample amount ACQ1 deltaic sand from fossil fluviatile-shallow marine setting from Crotone Basin, Southern Apennines.

Sampling strategy was aimed to collect sands with different modal compositions, average grain sizes and grain size distributions (different sorting degree, modal peak, curve shape and asymmetry). In particular, sample LIM1 was collected in a recent foreshore swashing zone along the eastern coast of Lemnos Island in the North Aegean Sea, Greece. The beach sand is medium-grained, well sorted, and displays high-textural maturity with rounded to subrounded grains mainly composed of quartz and lithic fragments (Fig. 2b). Three sand specimens were sampled from different braided stream type, creeks, of Northern Apennines in North Italy, with samples PAR1 and PAR2 representing the bottom and the top of a recent fluvial sand bar along the Parma Creek, respectively. The sand bar is interfingered with coarse gravel and boulder-cobble bodies. The sand samples are fine to medium-grained, with moderate sorting degree, fair textural maturity with subrounded grains composed of quartz, feldspar, and silt-clay aggregates (Fig. 2c and d). Conversely, PES1 sample was collected at the base of a recent slope debris talus slightly reworked by stream current along the Pessola Creek in the Northern Apennines. The sand exhibits medium to coarse grain size, moderate to poor sorting, and low textural maturity indicated by subrounded to subangular grains mainly composed of lithics and subsidiary quartz and feldspar (Fig. 2e). Eventually, ACQ1 sand sample was collected from a Lower Pliocene age deltaic sandstone bar from the Crotone Basin in South Italy. Although this sample belongs to a fossil siliciclastic deposit, the sandstone is almost devoid of any diagenetic cements, thus allowing an easy sampling. This fluvial-deltaic sandstone is coarse-grained, poorly sorted and displays low textural maturity, with subangular feldspar grains dominating with respect to rock fragments and quartz (Fig. 2f).

4.2 X-ray diffraction mineralogical analysis

The detailed analysis of the mineralogical composition of sampled sands was achieved through X-Ray Powder Diffraction (XRPD) technique. Before the analyses, all samples were dried at the controlled temperature of 35 °C for 48 hours and representative sand amounts (~2 g) were manually milled in a jade mortar to attain an average grain size < 63 µm. A Bruker D2 Phaser powder diffractometer with θ-θ focalizing geometry was used, operating at 30 kV and 10 mA with Cu-Kα (λ = 1.54178 Å) radiation. Data were collected in the 5-60° 2θ angular range, with 0.02° step size and 1 s/step counting time. Each sample was spun at 30 rpm. To identify the crystalline phases EVA software (Bruker EVA, 2018) and the

https://doi.org/10.5194/egusphere-2023-2636
Preprint. Discussion started: 15 November 2023

Crystallography Open Database (COD) were used. Semi-quantitative analysis of the detected mineralogical phases was conducted using the RIR method, adding a 10 wt% high purity Si standard in each sample. Through the adoption of semi-quantitative technique, the identification of clay minerals through emission peak position cannot be considered exhaustive. Further investigation and analysis of samples under different conditions (dry, heated, and swollen) would be required for a precise clay mineral identification but such in-depth analysis falls beyond the scope of the present study.

4.3 Laser-diffraction grain size analysis

All granular samples were dried into an oven at the controlled temperature of 40 °C for two days to remove most of the water content. After sample drying, the total amount (~500 g) was sieved with a 2,000 µm mesh to remove grains with equivalent diameter coarser than 3,500 µm, which represents the upper instrumental limit of the laser granulometer. By doing this, we slightly restricted the original grain size distribution of all samples, removing fine gravel sized grains. The alteration by sieving of original grain size distribution was the same for all samples. The original sample amounts were split in aliquots using Quantachrome Instruments macro and micro rifflers to achieve the sample mass required for grain size analysis (0.8-1.3 g) (Fig. 3a). This process allowed also to create sub-samples still preserving the original grain size distribution of the total starting sample amount. Grain size analyses were performed with a Malvern Panalytical Mastersizer 3000 optical granulometer, with operating size range spanning from 10 nm to 3,500 µm (Fig. 3b). The instrument was equipped with an Aero S air-dispersed analysis unit, using pressurized air as particle dispersant medium (Fig. 3b). The adoption of air as dispersant allowed to analyze samples minimizing the alteration and mechanical disaggregation operated by commonly used liquid dispersant media (distilled water or alcohol). For all five analyzed samples, a specific standard operating procedure was set to grant the most reliable and reproducible analysis.

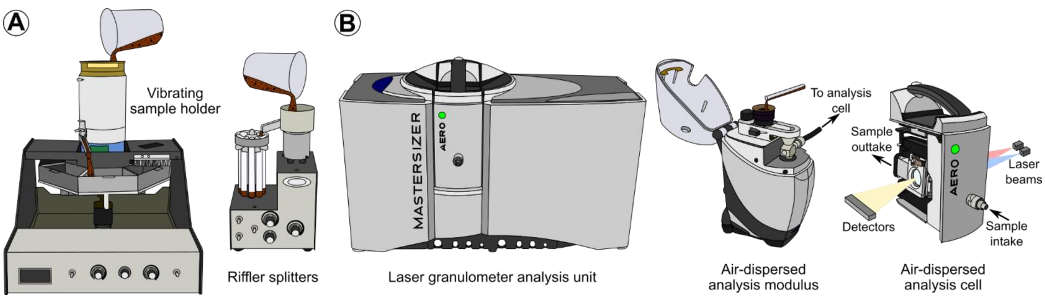

Figure 3. Instrumental apparatus and sample preparation used to perform laser diffraction analysis. (**a**) Macro and micro rifflers necessary to split the initial sample amount in sub-samples suitable to be inserted in the laser granulometer and to be dedicated to thin sectioning. (**b**) Mastersizer 3000 laser granulometer optical unit, equipped with an Aero S air-dispersion modulus with the dedicated analysis cell designed to work on incohesive granular media.

The operating procedures included several analytical-instrumental parameters to be set prior to the definitive analysis. In our analyses, the granular sample quantity, laser power obscuration, negative air pressure and feed rate were carefully tested (details are provided in Supplementary material 1). The granulometer has two different light sources producing two laser beams with red (632.8 nm) and blue (470 nm) wavelength, respectively (Fig. 3b). Calculation of the equivalent grain diameter was made via a light diffraction law, employing the Mie light scattering theory, which requires the refractive and adsorption indexes of particles. Our granular materials are multi-dispersed (particles with different size and shape) mixtures of several mineralogical phases including quartz, K-feldspar, plagioclase, mica, and rock fragments in different proportions. Nevertheless, we adopted the optical parameters of crystalline quartz, which is the most abundant mineral phase, with diffraction index of 1.54 and adsorption index of 0.1. This simplification was needed because the granulometer is not designed to work on complex polymineralic assemblages. Particle volume was back-calculated from light diffraction scattering distribution and, under the assumption of perfect spherical objects, the equivalent diameter was calculated. Optical diffraction is operated differently according to grain size, with fine particles producing wide light scattering angles, while coarse grains induce low angles (Brooks et al., 2022). The laser granulometer performs the calculation of equivalent grain diameter adopting the method of moments as indicated in the generic formula below:

$$D[m,n] = \left(\frac{\sum_{i=0}^{i=n} V_i * d_i^{m-3}}{\sum_{i=0}^{i=n} V_i * d_i^{n-3}}\right)^{\frac{1}{m-n}} \quad (5)$$

in which V_i stands for particle volumetric density in size class d_i (median value of grain size class), while *m* and *n* are the exponents to be substituted with different indexes according to the adopted method of moments. In our case, the granulometer calculates the volume-weighted mean diameter (De Broucker mean diameter or D[4:3]), adopting as indexes *m* and *n* in equation 5, 4 and 3, respectively. The granulometer also provides the span, or the width of the grain size distribution curves calculated at half height of modal peak, according to the formula:

$$Span = \frac{d(x,0.9) - d(x,0.1)}{d(x,0.5)} \quad (6)$$

where, *d* is the equivalent particle diameter value at 0.1, 0.5 and 0.9 thresholds of the grain size distribution, and *x* can be substituted according to the distribution type adopted during the analysis (number or volume of particles). Optical granulometric analyses were replicated on 5 aliquots of each sample. Grain size distribution curves were averaged to obtain mean grain diameters and related parameters with associated standard deviations.

4.4 Thin sectioning technique of loose sand samples

https://doi.org/10.5194/egusphere-2023-2636
Preprint. Discussion started: 15 November 2023

Petrographic thin sections having thickness of 30 µm were made from granular sand samples. To prevent any preferential grain orientation and to preserve the original grain size distribution, all samples were split with macro and micro rifflers, and several aliquots were added into Teflon containers (Fig. 4a).

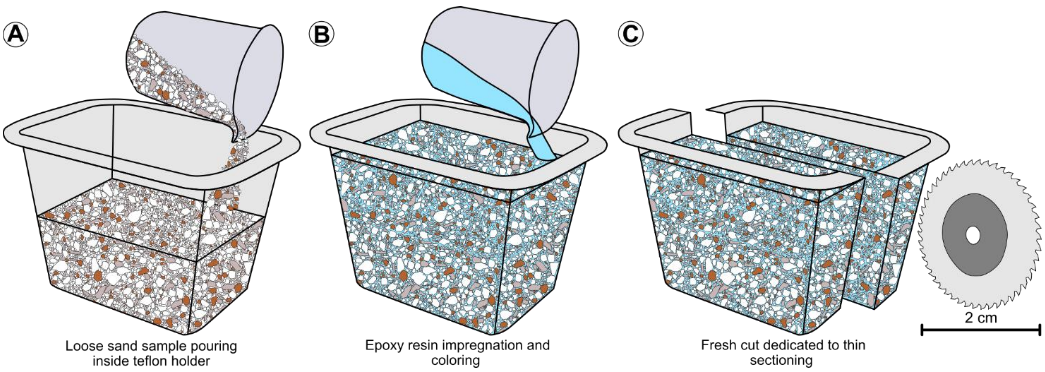

Figure 4. Sample preparation before thin sectioning. (**a**) Sample pouring inside Teflon holder after being split in representative sub-samples with vibrating rifflers. (**b**) Granular sample impregnation with a mixture of Araldite resin and Prochima Pentasol blue dye. (**c**) Precise saw-cutting along the vertical direction, with thin section made along the fresh cut.

Typically, 20-28 g of loose sand were used to fill 4 × 3 × 2.5 cm Teflon sample holders, with mass variations due to different sample density and grain size. Loose sand samples were impregnated with a mixture of Araldite BY156 epoxy resin and Aradur 21 resin hardener (resin-hardener mass proportion of 100:28), which was diluted to 10% of total volume with ethyl acetate to grant lower viscosity. The mix was colored by adding a Prochima Pentasol (UN) blue dye with a mass equal to 6% of the Araldite resin (Fig. 4b). The coloring provided a uniform light blue background which helped in identifying grains and tracing grain boundaries. Indurated samples were cut vertically, and the fresh cut was used to create petrographic thin sections (Fig. 4c). Thin rock slices were glued onto transparent glass adopting an Epoteck 301 epoxy resin mixed with Aradur 21 hardener (resin-hardener mass proportion of 20:5). Eventually, thin sections were manually polished with polycrystalline synthetic diamond powder, having a grain size of 1 µm, above a Tanganyika soft wooden surface. The polishing procedure was needed to precisely identify grain mineralogy, to detect grain outer boundaries and to increase the overall thin section transparency and quality.

4.5 Sand sample modal composition

The definition of the modal composition of sand samples was obtained by means of petrographic analysis, with recognition of the principal mineralogical phases (quartz, feldspar, and lithic fragments) in thin section. Quantification of areal percentage of minerals was done on high resolution photomicrographs acquired with a Zeiss Axioplan 2 petrographic microscope, equipped with a Leica MC 170 HD high sensitivity camera. Photomicrographs were acquired at 12.5× magnifications (picture area of 4,747 × 3,560 µm) both under plane and cross polarized light, to ease mineral identification. A total of 5 dedicated photomicrographs were taken and analyzed for each sample. Sand samples were classified adopting the standard Q-F-L ternary classification diagram used for sandstones (Folk, 1974).

4.6 Particle size analysis through 2D image analysis

The analysis of grain size via image analysis on thin section was performed on petrographic photomicrographs acquired with the standard microscope setting described above. For each thin section, 48 to 64 photomicrographs were taken at 12.5× magnifications (picture area of 4,747 × 3,560 µm) under plane polarized light to cover the entire thin section area and were stitched together to form photomosaics. Photomosaics were imported and calibrated in

https://doi.org/10.5194/egusphere-2023-2636
Preprint. Discussion started: 15 November 2023

ImageJ image analysis, open-source software (Schneider et al., 2012). Little processing was required to enhance image quality mainly through brightness-contrast adjustments and noise-outlier pixel removal (Fig. 5a).

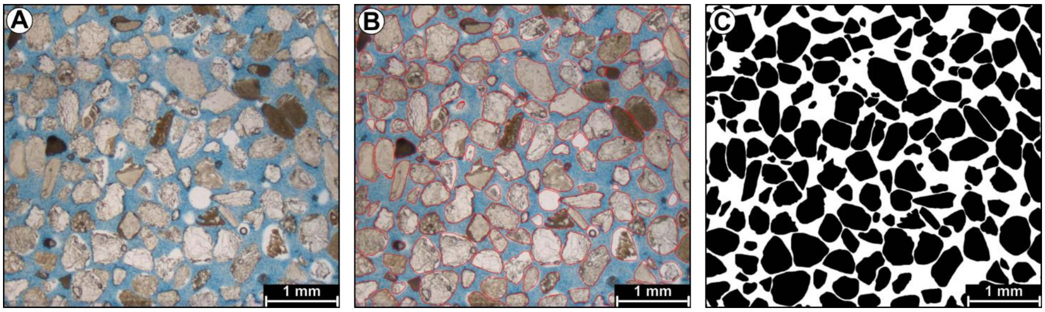

Figure 5. Image analysis technique adopted to obtain 2D particle size distribution from the selected samples. (**a**) Original photomicrograph acquired at 12.5× magnification, composing the analyzed photo-mosaics. (**b**) Results of manually traced particle outer boundaries. (**c**) Transformed binary (black and white) photomicrograph used to extract particle equivalent diameter.

Grains were traced on modified photomosaics with ImageJ manual tracing tool, having care to keep a constant 2-pixel width of the traced boundaries (Fig. 5b). After digitization, grains were identified by the software with color thresholding technique applied to red grain boundaries and photomosaics were converted to binary images (black grains on white background) (Fig. 5c). Special attention was paid in drawing grain boundaries, to avoid grains in contact with each other. In the case of touching grains, instead of operating image segmentation, we preferred double-checking the results to find errors and mistakes during tracing, that were corrected by manual separation of grains adding different color pixels (Fig. 6).

https://doi.org/10.5194/egusphere-2023-2636
Preprint. Discussion started: 15 November 2023

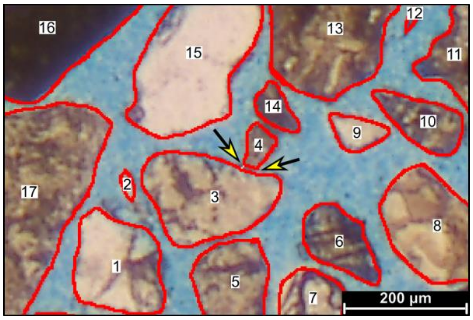

Figure 6. Double-checking of grains in contact with each other. Final digitized photo-mosaics quality check to identify tangent grains which were manually segmented by adding pixels with different color from the red particle outline (yellow arrows).

After image correction, grain size-shape data were extracted. For grain size, we extracted the area fraction in µm^2 of grains which were approximated to perfect circles, and the equivalent diameters were calculated from the inverse formula of the circle's area (Fig. 7):

$$d_{eq} = 2 * \sqrt{\frac{A}{\pi}} \tag{7}$$

where d_{eq} is the equivalent diameter of the circle having the same area of the particle and A is the real area of the particle measured with image analysis.

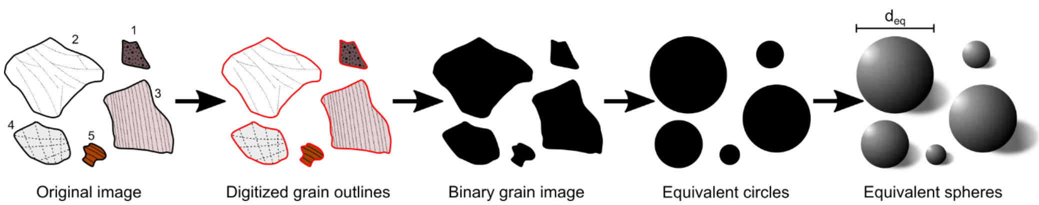

Figure 7. Sequence of progressive steps to perform manual image analysis and to extract particle equivalent circles and spheres. d_{eq}, equivalent particle diameter.

Values extracted from this formula composed the basis of the proposed volume-weighted mean diameter. A total of 133,372 grains were considered and typically more than 5,000 grains were used in each thin section. Large datasets allowed to tune the volume-weighted calculation formula and to minimize the effect of random grain sectioning (Krumbein, 1935;

https://doi.org/10.5194/egusphere-2023-2636
Preprint. Discussion started: 15 November 2023

Friedman, 1958; Kellerhals et al., 1975; Kong et al., 2005). Grain size distributions were created from the conversion of particle number into volume density percentage associated with each grain size bin. Conversion was made considering the total volume of spherical-shape grains divided according to the instrumental grain size classes adopted by the laser granulometer. By doing this, we kept the same boundary and instrumental conditions for both grain size data acquired through laser granulometry and image analysis, facilitating the comparison.

Regarding grain shape, aspect ratio (AR) was calculated and used to describe the deviation of grains with respect to the perfect circle. Aspect ratio was obtained by the formula:

$$AR = \frac{Major\ axis}{Minor\ axis} \quad (8)$$

where *Major axis* indicates the longest axis of the particle best fit ellipse (segment connecting the two farthest points along the grain perimeter) and *Minor axis* stands for the shortest axis of the best fit ellipse (segment having as tips the two closest points along the grain perimeter).

5. Main results

5.1 Petrographic-mineralogical sample description

Micro-textural and modal analyses performed on the foreshore beach sand sample (LIM1), point out a mineralogical composition made of almost equal proportions of quartz (38.81-53.32%) and lithic fragments (32.05-46.8%), while feldspar and plagioclase are subordinate (8.37-20.17%) (Fig. 8a and b). Lithic fragments are mainly composed of calcite-aragonite bioclasts, peloids, and to a lesser extent of metamorphic and igneous rock fragments. This sample plots between the feldspathic litharenite and litharenite compositional fields in the

https://doi.org/10.5194/egusphere-2023-2636
Preprint. Discussion started: 15 November 2023

Q-F-L classification diagram (Fig. 8a). Grains are rounded to subrounded, with quartz being more equant than feldspar and lithics which appear more elongate. Sorting degree is high with grains of different mineral composition showing similar overall size.

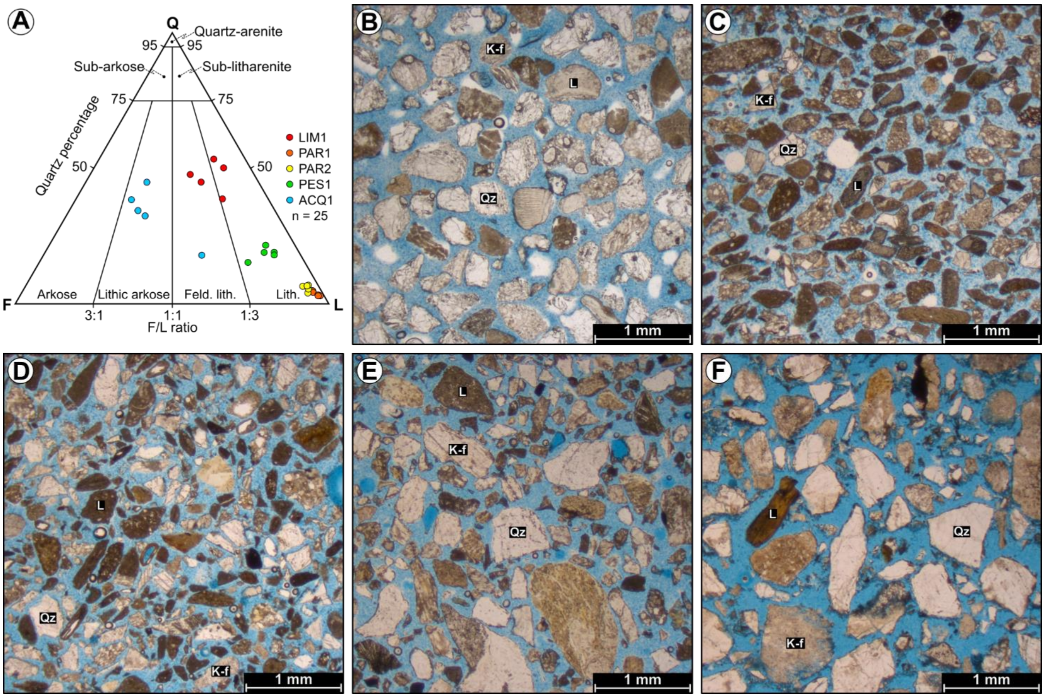

Figure 8. Micro-textural characteristics and mineralogical composition of the collected sand samples. (**a**) Ternary Quartz-Feldspar-Lithics modal classification diagram reporting the composition of studied sands (Folk, 1974). Sand composition was calculated from 5 photomicrographs per each sample. (**b**) Rounded to subrounded siliciclastic and biogenic particles composing LIM1 beach sand sample. (**c**) Subrounded and elongate lithic-dominated grains of PAR1 fluvial sample. (**d**) Subrounded lithic-dominated particles with lesser extents of quartz and feldspar composing PAR2 fluvial sample. (**e**) Subangular and poorly sorted fluvial sand of PES1 sample. (**f**) Angular to subangular, poorly sorted fluvial-deltaic sand composing ACQ1 sample. Q, quartz; K-f, feldspar; L, lithic fragment; n, number of used photomicrographs.

Sand sample collected along the base of a fluvial bar (PAR1), displays a completely different mineral assemblage compared to the latter beach sand. In particular, the modal analysis returns a high lithic percentage (92.75-95.74%), while quartz (3-4.51%) and feldspar (1.25-2.86%) compose the remaining areal amounts of the sample (Fig. 8a, c). Lithics have a sedimentary origin with silt-clay aggregates incorporating fine-grained quartz and feldspar particles to produce coarse-grained aggregates. The fine-grained matrix of aggregates is dominantly composed of muscovite and chlorite-group minerals, as confirmed by XRD analysis. Metamorphic and igneous fragments are present as subordinate mineral components. Due to the high lithic content, PAR1 sample can be inserted in the litharenite field in the Q-F-L ternary diagram, close to the 100% lithic endmember (Fig. 8a). Grains are generally subrounded, with lithics exhibiting more anisotropic shapes with smooth outer boundaries, while quartz grains are subangular with rougher boundaries. The sorting degree is average with grains covering different grain size classes.

The sample from the top of the fluvial bar (PAR2), shows a mineral composition close to the underlying PAR1 previously described, with lithics dominating with respect to quartz and feldspar. Lithic fragments compose most of the areal percentage of the sample (88.65-91.36%), while quartz (4.01-6.72%) and feldspar-plagioclase (3.22-4.84%) are subordinate (Fig. 8a, d). Lithics are mainly made of sedimentary aggregates of silt and clay-sized particles (muscovite and chlorite), but a lesser content of metamorphic rock fragments occurs (polycrystalline quartz grains). This sample can be inserted in the litharenite, lithic-dominated field in the Q-F-L ternary diagram, next to PAR1 sample (Fig. 8a). Lithic fragments are subrounded with highly elongate shapes and smooth boundaries. Conversely, quartz grains are subangular to angular with marked asperities and edges along the outer boundaries. Feldspar and plagioclase are subrounded and grains display smooth perimeters. The sorting of the sample is average with a considerable span through grain size classes.

The fluvial-reworked talus debris sample (PES1) is characterized by a mineral composition shifted towards lithics, with considerable amounts of quartz and feldspar. Again, lithic fragments constitute more than half of the sample (66.44-73.57%), followed by quartz (15.5-

https://doi.org/10.5194/egusphere-2023-2636
Preprint. Discussion started: 15 November 2023

21.62%) and feldspar-plagioclase (7.96-18.05%) (Fig. 8a, e). Most of lithics are composed of ultramafic rock fragments (basalts, peridotites and gabbros), with lesser contribution from metamorphic, hydrothermally altered rocks (serpentinites). Sedimentary lithic aggregates of silt and clay, encasing siliciclastic particles, occur. The fine-grained matrix forming aggregates is composed of clay minerals as documented by XRD analysis (Supplementary material 2). According to the Q-F-L ternary diagram, PES1 sample can be ascribed to the litharenite field, although slightly enriched in quartz and feldspar with respect to PAR1 and PAR2 (Fig. 8a). Lithic fragment shape varies from subrounded to angular, with very rough outer boundaries. Feldspar grains show subrounded and isotropic crystal form, while quartz has subangular to angular shape. The sorting degree is poor, with particles displaying a wide grain size span.

Eventually, the sand sample collected from the deltaic sandstone bar (ACQ1) displays a mineral composition with similar percentage of feldspar, quartz and lithics. In this sample, feldspar and plagioclase compose most of the sample (31.58-43.81%), followed by quartz (18-44.83%) and lithic fragments (17.9-50.41%) (Fig. 8a, f). Lithics have different composition, with igneous-intrusive terms (granites) dominating with respect to metamorphic (schists-gneisses) and sedimentary ones (sandstones). Feldspar and plagioclase crystals are severely affected by alteration to sericite minerals (muscovite and paragonite). ACQ1 sample can be inserted in the lithic arkose field of the Q-F-L classification diagram (Fig. 8a), although one of the used photomicrographs falls in the feldspathic litharenite field due to the heterogeneous distribution of several coarse feldspar grains. Feldspar grains have subrounded shape, while quartz is subangular to angular. Lithic fragments of igneous origin have subangular shape with rough outer boundaries, while sedimentary lithics are subrounded and more elongate, with smooth boundaries. The sorting degree is low, with a wide span of grain size classes.

https://doi.org/10.5194/egusphere-2023-2636
Preprint. Discussion started: 15 November 2023

5.2 Laser-diffraction grain size analysis

Optical granulometry grain size analyses on loose samples were replicated with 5 aliquots of equal mass, and the grain size distribution curves were averaged to obtain a mean grain diameter value and related parameters. The following results are presented considering the calculated average grain size distribution curve for each sample.

5.2.1 Beach sand sample (LIM1)

LIM1 sample displays a narrow grain size distribution curve, with subtle positive asymmetry. The grain size distribution has intercepts with X axis at 174 and 1,041 µm, respectively. The calculated average grain diameter is 434 ± 2.3 µm, with a modal value of 419 ± 1.9 µm and a median of 420 ± 1.9 µm (Fig. 9a). The span of grain size distribution is low (good sorting degree) with an average value of 0.665 ± 0.01. All grains fall in the sand grain size interval with the most recurrent size class being the medium-grained sand with 72.91% of particle volume density. Coarse-grained particles compose 25.26% of the total sample volume, while the remaining 1.83% is due to the fine-grained sand fraction (Fig. 9a).

5.2.2 Basal fluvial sand bar sample (PAR1)

The sand sample collected along the basal surface of a fluvial sand bar along the braided-stream Parma Creek (PAR1), is characterized by an average grain size distribution curve with medium width showing positive asymmetry. The left (finer) tail of the distribution curve is more pronounced than the right (coarse) one with particles being detected at 2.9 µm on the fine-ward side. Conversely, the right tail of the grain size curve intercepts the X axis at 1,182 µm. The average particle diameter is 352 ± 3.9 µm, with a modal value of 350 ± 1.9 µm and a median of 328 ± 2.6 µm (Fig. 9b). Grain size distribution span is higher than the

https://doi.org/10.5194/egusphere-2023-2636
Preprint. Discussion started: 15 November 2023

one shown by the previous sample and the calculation returns a mean value of 1.343 ± 0.02. The most recurrent grain size class is the medium-grained sand with 50.89% of particle volume density. Fine-grained and coarse-grained classes compose 22.93% and 18.79% of the total sample volume, respectively. Minor amounts of volumetric densities are measured in the silt size (4.07%), very fine-grained sand size (3.08%), and in very coarse-grained sand size (0.15%) (Fig. 9b).

https://doi.org/10.5194/egusphere-2023-2636
Preprint. Discussion started: 15 November 2023

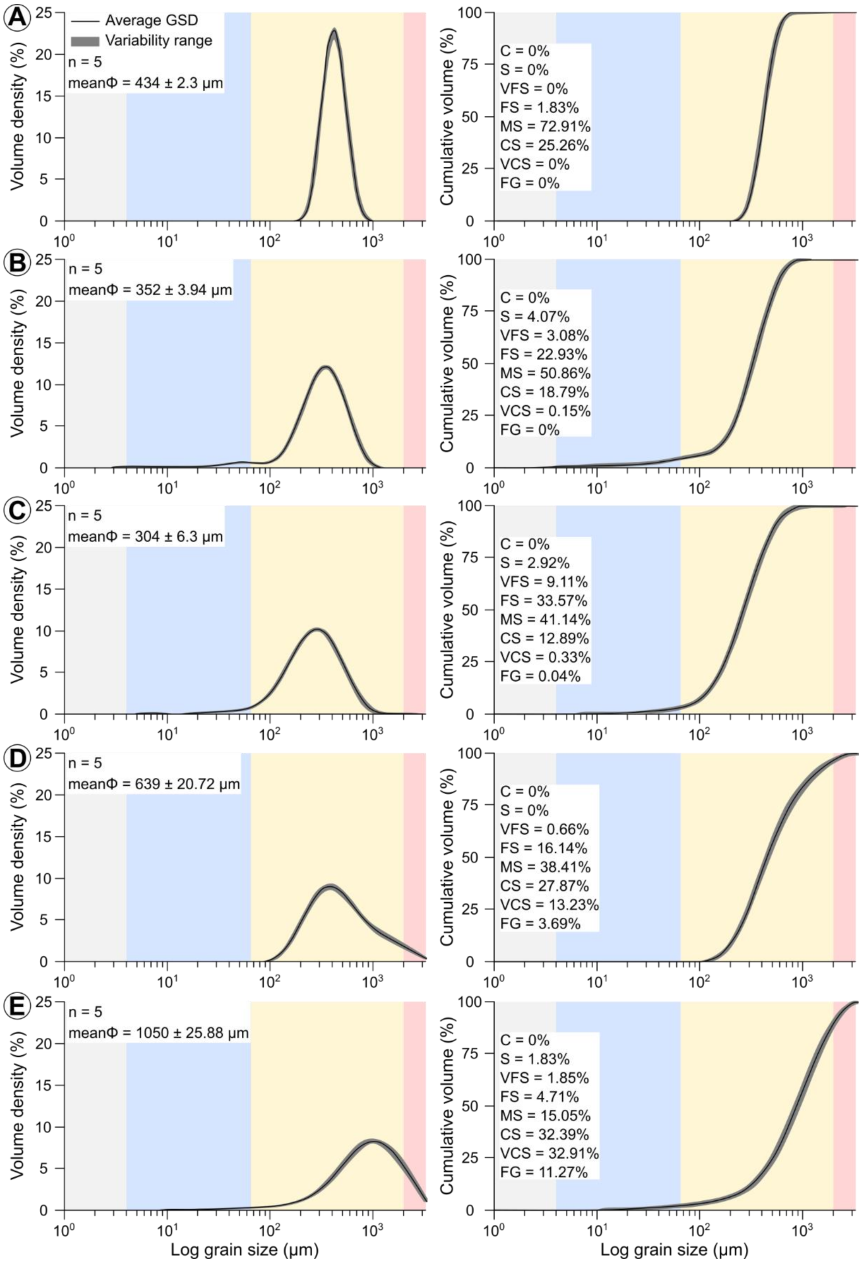

Figure 9. Grain size distribution curve obtained through laser granulometer analysis. (**a**) Volume density and cumulative distribution for LIM1 sample. (**b**) Volume density and cumulative distribution for PAR1 sample. (**c**) Volume density and cumulative distribution for PAR2 sample. (**d**) Volume density and cumulative distribution for PES1 sample. (**e**) Volume density and cumulative distribution for ACQ1 sample. GSD, grain size distribution; Φ particle diameter; n, number of analyses; C, clay; S, silt; VFS, very fine-grained sand; FS, fine-grained sand; MS, medium-grained sand; CS, coarse-grained sand; VCS, very coarse-grained sand; FG, fine

https://doi.org/10.5194/egusphere-2023-2636
Preprint. Discussion started: 15 November 2023

gravel.

5.2.3 Upper fluvial sand bar sample (PAR2)

The medium-grained sand collected on the top surface of a sandy bar along the Parma Creek (PAR2), displays an average grain size distribution curve with medium width and slight positive skewness. On the left tail, finest particles are recorded at 4.9 µm, while on the right tail coarsest grains are detected at 1,343 µm. The calculated average grain diameter is 304 ± 6.3 µm, with a mode at 286 ± 3.3 µm (Fig. 9c). The span of the average grain size curve is higher than previous samples, with a mean value of 1.608 ± 0.03 and a median of 267 ± 2.7 µm. Higher span is recorded also by the particle volume distribution, with 41.14% of grains falling in the medium-grained sand class and 33.57% of grains composing the fine-grained sand size. A considerable volume of particles falls in the coarse-grained sand size (12.89%), while only a small fraction is recorded in the very coarse-grained sand (0.33%) and fine gravel grain size classes (0.04%). On the fine-ward side, no clay-sized particles are recorded, while silt-size and very fine-grained sand classes compose 2.92% and 9.11% of the total sample volume, respectively (Fig. 9c).

5.2.4 Fluvially-reworked debris talus sand sample (PES1)

The medium to coarse-grained sand sample collected from a debris talus reworked by river stream (PES1) is characterized by an average grain size distribution curve with high width and strong positive asymmetry. Grain size distribution tails are not symmetric, with the left one being steeper than the right tail. On the left tail, finest grains are recorded at 81 µm, while on the right tail coarsest particles reach 3,300 µm of equivalent diameter. The average grain diameter gained from the mean curve is 639 ± 20.72 µm, with a modal value of 386 ± 2.41 µm and a median of 455 ± 8.6 µm (Fig. 9d). The span of average grain size curve is higher than the samples described before, with a mean value of 2.495 ± 0.11 µm. Higher span can be traced also in the volumetric particle distribution among grain size classes. In

https://doi.org/10.5194/egusphere-2023-2636
Preprint. Discussion started: 15 November 2023

particular, the dominant grain size class is the medium-grained sand size with 38.41% of volume density. Relatively high particle volumes are recorded also in the coarse-grained sand (27.87%), fine-grained sand (16.14%) and in the very coarse-grained sand classes (13.23%). Minor amounts of grains can be detected in the fine gravel class (3.69%) and in the very fine-grained sand range (0.66%) (Fig. 9d).

5.2.5 Deltaic sand sample (ACQ1)

The coarse-grained sandstone collected along an exposed fossil deltaic bar (ACQ1) displays a wide grain size distribution curve with a weak positive asymmetry. The average curve shows asymmetric tails, with a steep right tail (coarse) and a gentle left tail (fine). Finest particles are recorded at 8.1 µm, while coarse ones have equivalent diameters of 3,300 µm. The average equivalent grain diameter is 1,050 ± 25.88 µm, with a mode of 1,020 ± 57.92 µm and a median of 897 ± 27.1 µm (Fig. 9e). The span shown by the mean granulometric curve is equal to 1.993 ± 0.02 µm, slightly lower than PES1 sample. Data regarding single grain size classes point out the high curve width. In this sample is difficult to identify a single dominant grain size class, since coarse and very coarse-grained classes compose 32.39% and 32.91% of total volumetric particle density, respectively. Considerable particle amounts are also displayed by medium-grained sand (15.05%) and fine gravel size classes (11.27%). Minor volumetric densities are recorded in fine-grained sand range (4.71%), very fine-grained sand class (1.85%) and in the silt grain size interval (1.83%). No grains have been measured in the clay-sized fraction (Fig. 9e).

To summarize, from sample LIM1 to ACQ1 we record a coarsening of average grain diameter, a general broadening of grain size distribution curves (decrease of sorting degree), and a more marked asymmetry between left and right tails of the curves (Fig. 10a and table 1). The same observations can be made checking the cumulative grain size

https://doi.org/10.5194/egusphere-2023-2636
Preprint. Discussion started: 15 November 2023

distributions, which show a progressive decrease of slope following an increase of grain size (Fig. 10b and table 1).

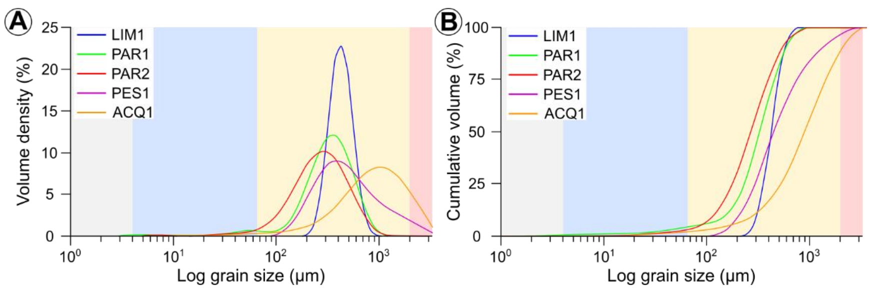

Figure 10. Comparison of grain size distribution obtained with air-dispersed laser granulometer. (**a**) Volume density grain size distributions. (**b**) Cumulative volume percentage grain size distributions.

Table 1: Summary of analytical parameters extracted from laser granulometry analyses

Sample name	Sample type	Age	D_m (μm)	D_{x10} (μm)	D_{x50} (μm)	D_{x90} (μm)	Mode (μm)	Span
LIM1	Foreshore beach sand	Recent	434 ± 2.3	303 ± 1.87	420 ± 1.92	582 ± 4.15	419 ± 1.94	0.665 ± 0.01
PAR1	Base of fluvial sand bar	Recent	352 ± 3.94	152 ± 1.48	328 ± 2.61	593 ± 9.76	350 ± 1.92	1.343 ± 0.02
PAR2	Top of fluvial sand bar	Recent	304 ± 6.3	115 ± 1.34	267 ± 2.68	545 ± 12.18	286 ± 3.29	1.608 ± 0.03
PES1	Talus debris reworked along river	Recent	639 ± 20.72	211 ± 1.92	455 ± 8.62	1350 ± 71.55	386 ± 2.41	2.495 ± 0.11
ACQ1	Deltaic sandstone bar	Lower-Middle Pliocene	1050 ± 25.83	283 ± 8.02	897 ± 27.14	2070 ± 40.86	1020 ± 57.92	1.993 ± 0.02

Table 1. Summary of grain size analysis via laser granulometry. D_m, average particle diameter; D_{x10}, D_{x50}, D_{x90}, grain size thresholds (percentiles) at 10, 50 and 90% of particle volume distribution.

5.3 Thin section-image analysis grain size distributions

Two-dimensional grain size analysis was based on data gained from petrographic thin sections analyzed through image analysis technique. All grains composing the thin sections were digitized to provide robust datasets which served to set the 3D volume-weighted mean diameter conversion formula (Fig. 11).

5.3.1 Beach sand sample (LIM1)

https://doi.org/10.5194/egusphere-2023-2636
Preprint. Discussion started: 15 November 2023

For the foreshore-beach sand sample LIM1, a total of 5,419 grains were acquired (Fig. 11a). The resulting particle number grain size distribution curve has intercepts with the X axis at 40 and 756 µm and a mode of 352 µm. The volume density converted distribution shows a roughly symmetric bell shape with a weak skew towards finer particles and a modal value of 390 µm (Fig. 12a). The sorting degree is high as testified by most of the grains falling in the medium-grained sand size class (87.54%), while lesser particle amounts are recorded in the fine-grained sand (6.89%) and in the coarse-grained sand intervals (5.29%). Only small fractions of silt-sized and very fine-grained sand material were detected, with percentage of 0.01% and 0.26%, respectively (Fig. 12a).

https://doi.org/10.5194/egusphere-2023-2636
Preprint. Discussion started: 15 November 2023

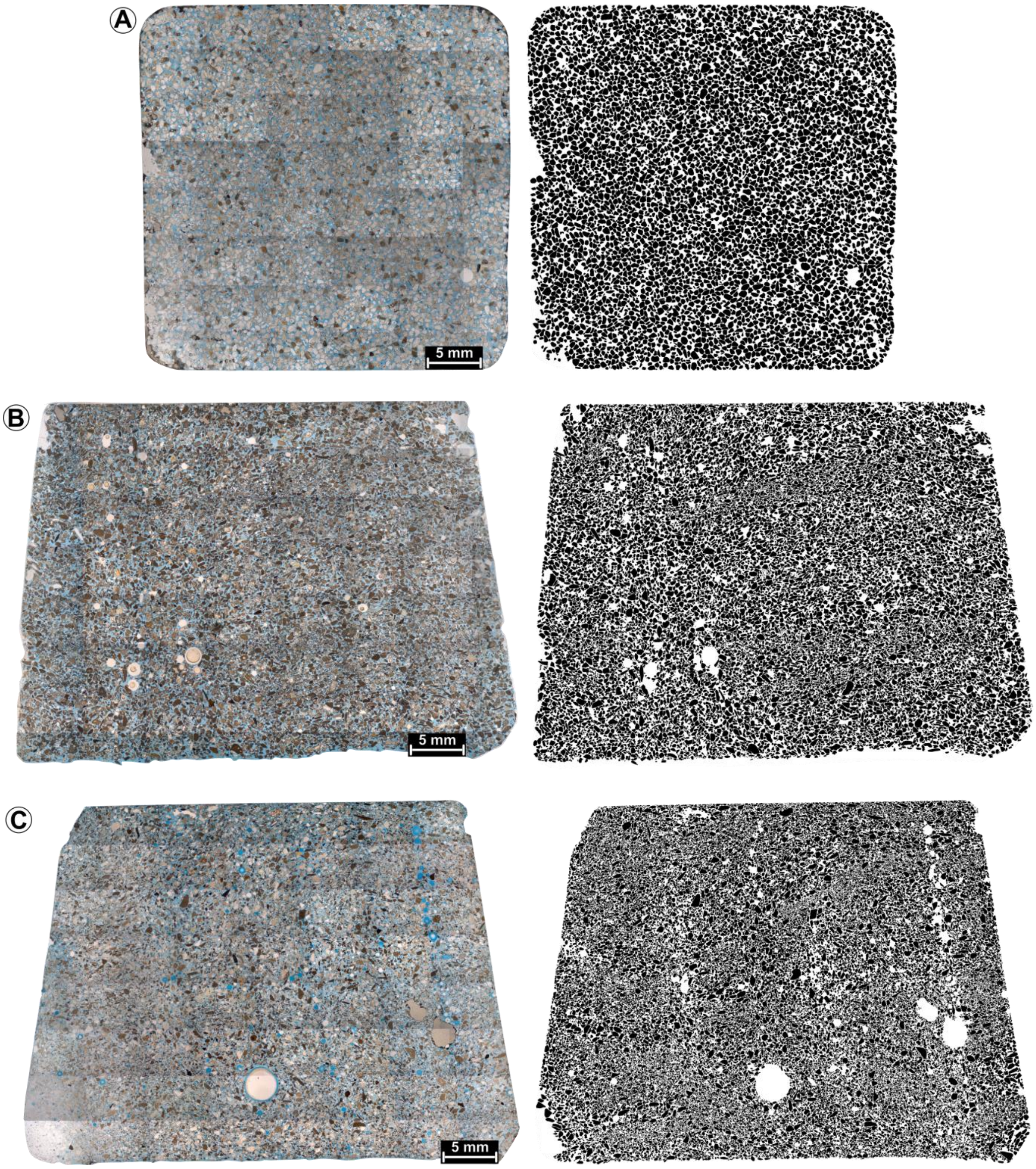

Figure 11. Original and binary photo-mosaics of the analyzed thin sections composed of tens of photomicrographs stitched together. (**a**) LIM1 beach sample. (**b**) PAR1 fluvial sample. (**c**) PAR2 fluvial sample. (**d**) PES1 fluvial sample. (**e**) ACQ1 fluvial-deltaic sample.

5.3.2 Basal fluvial sand bar sample (PAR1)

https://doi.org/10.5194/egusphere-2023-2636
Preprint. Discussion started: 15 November 2023

The fluvial sand bar sample PAR1 was analyzed by acquisition of 20,105 grains (Fig. 11b). The particle number distribution describes a "bell-shape" curve, with the finest grains recorded at 16.4 µm, coarsest ones at 859 µm and a mode of 186 µm. The density volumetric distribution is described by a slight left asymmetry with a modal peak at 310 µm (Fig. 12b). Sorting is lower compared to LIM1 sample, with a broader grain size distribution as can be observed by particle volume density distribution through standard grain size classes. The dominant size class is the medium-grained sand composing 59.04% of the sample volume, followed by the fine-grained sand constituting 32.81% of volume density. Lesser amounts of very fine-grained sand (3.32%) and coarse-grained sand (4.49%) have been detected. Silt-sized material composes only 0.33% of the analyzed sample (Fig. 12b).

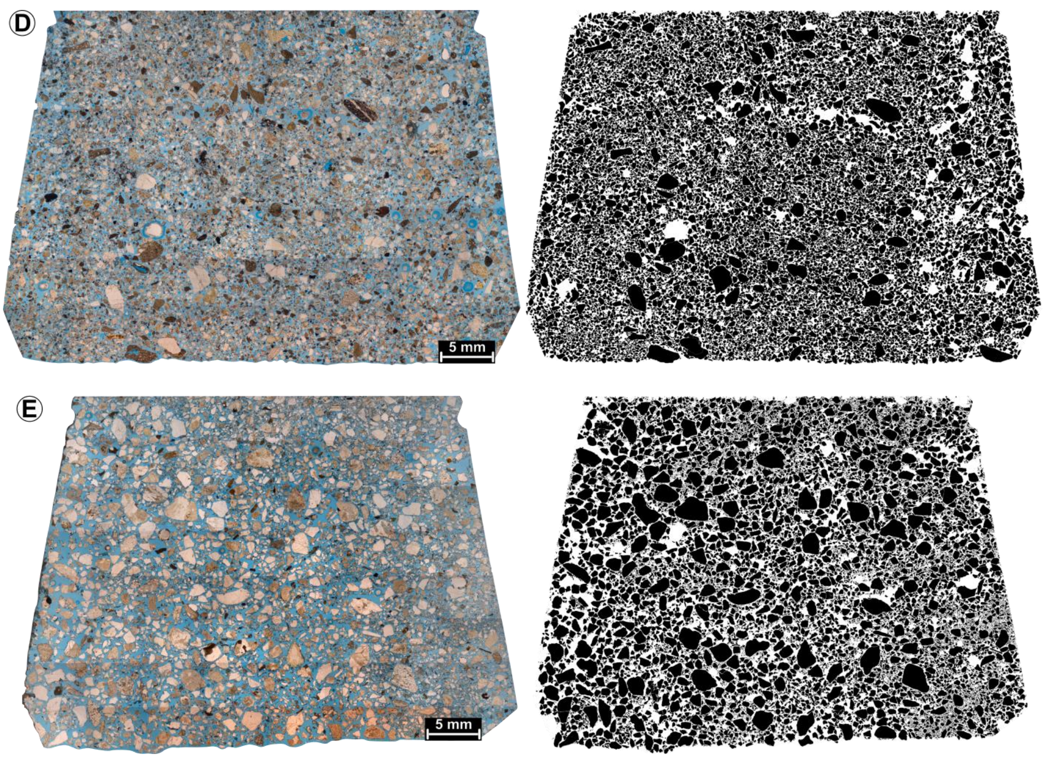

Figure 11 continued.

https://doi.org/10.5194/egusphere-2023-2636
Preprint. Discussion started: 15 November 2023

689 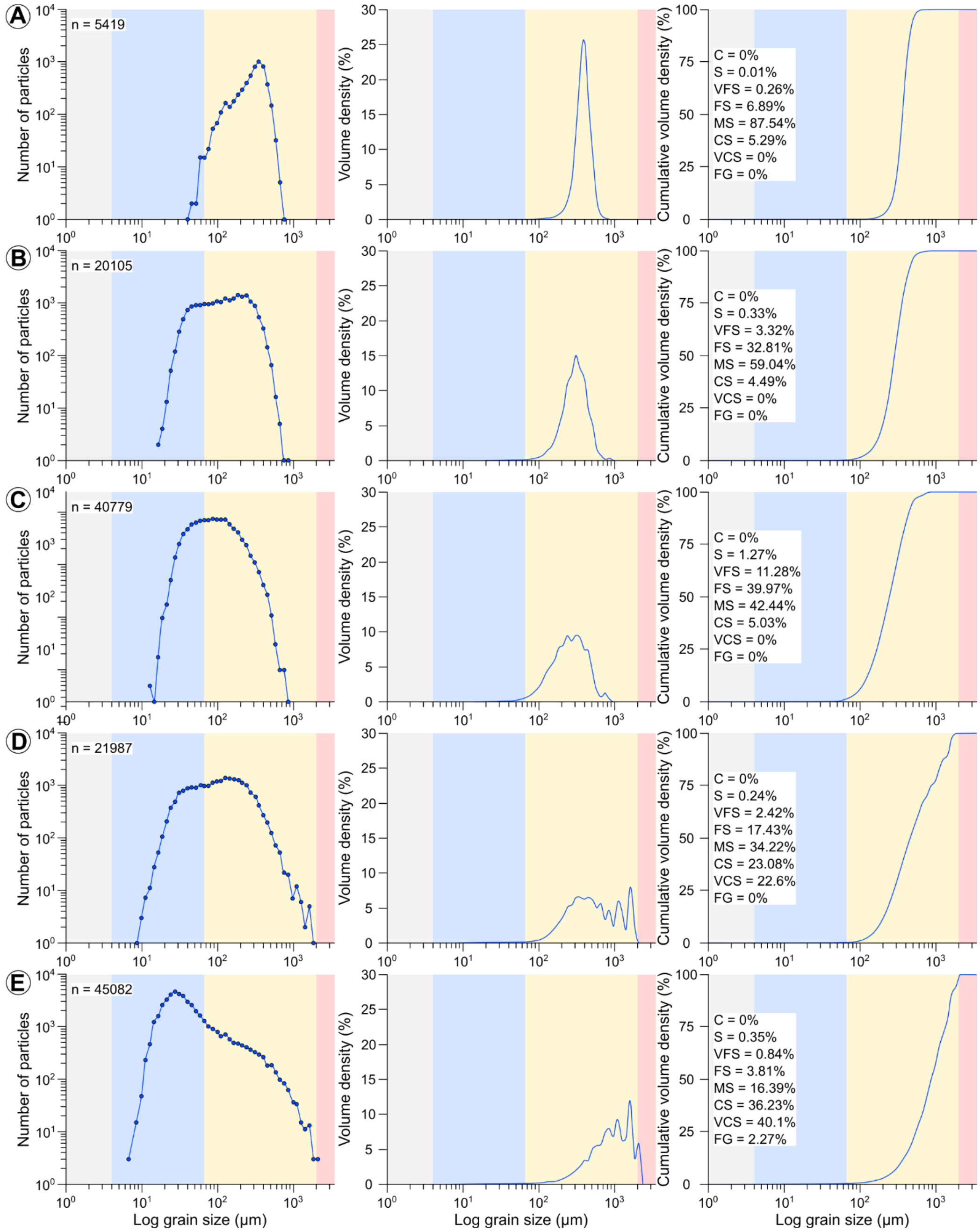

690 **Figure 12.** Grain size distribution curves extracted from 2D thin sections through image analysis. Results are
691 presented as number of particles, volume density and cumulative volume percentage distributions. (**a**) LIM1
692 beach sample. (**b**) PAR1 fluvial sample. (**c**) PAR2 fluvial sample. (**d**) PES1 fluvial sample. (**e**) ACQ1 fluvial-
693 deltaic sample. n, number of particles. C, clay; S, silt; VFS, very fine-grained sand; FS, fine-grained sand; MS,

https://doi.org/10.5194/egusphere-2023-2636
Preprint. Discussion started: 15 November 2023

medium-grained sand; CS, coarse-grained sand; VCS, very coarse-grained sand; FG, fine gravel.

5.3.3 Upper fluvial sand bar sample (PAR2)

40,779 grains were obtained from the second fluvial sand bar sample PAR2 (Fig. 11c). The distribution of particle number is characterized by a symmetrical bell-shaped curve with finest recorded particles at 12.7 µm, equivalent diameter of coarsest grains up to 859 µm and a modal value of 86.4 µm. Although we defined one single modal value, the modal peak described is wide and most of the grains have equivalent diameter falling between 58.9 and 127 µm. Data converted in particle volume density show a left asymmetry of the distribution curve and a modal peak at 310 µm (Fig. 12c). The width of the curve (i.e., sorting degree) is higher than the previous samples. Grains are almost equally distributed between the medium and fine-grained sand size classes, with volume densities of 42.44% and 39.97%, respectively. Significant particle volume is recorded in the very fine-grained sand size class (11.28%), while only 5.03% of particles fall in the coarse-grained sand interval. Silt-sized material composes 1.27% of the total sample volume (Fig. 12c).

5.3.4 Fluvially-reworked debris talus sand sample (PES1)

PES1 sample, the reworked debris talus along the river stream, was analyzed by considering a total of 21,987 grains (Fig. 11d). The distribution by number of particles describes a wide, almost symmetrical bell-shape, having as lower and higher intercepts with X axis at 8.68 and 1,850 µm, respectively. The modal peak is broad, with most recurrent data in between 111 and 240 µm size interval and a modal value of 127 µm. The volume density corrected curve displays a left asymmetry with a modal peak of 352 µm and a right curve tail with oscillating volume density associated with coarser particles (Fig. 12d). The sorting degree is low as indicated by the width of the modal peak. The volume density curve has a high width, testified by the significant spread of particles in different grain size classes. In particular, the most recurrent size class is the medium-grained sand interval with 34.22% of total grains, followed by the coarse-grained sand class composing 23.08% of the sample. Significant volume densities of very coarse-grained and fine-grained sand are documented, with percentages of 22.6% and 17.43%, respectively. Small volume of very fine-grained sand material is recorded (2.42%), together with silt-sized particles (0.24%) (Fig. 12d).

5.3.5 Deltaic sand sample (ACQ1)

Two-dimensional grain size of ACQ1 sample, collected along a fossil deltaic bar, was investigated with a total amount of 45,082 grains (Fig. 11e). The number of grain distribution highlights an asymmetric shape with right skew, and finest particles recorded at 6.72 µm and coarsest ones at 2,100 µm. The modal value of the distribution lies in the fine-grained interval at 27.4 µm. The volume density distribution curve displays a left asymmetry, with a gentle left tail and a steep right tail showing marked data oscillations. The modal peak is located at 1,630 µm in the coarser end of the distribution curve and the sorting degree is low (Fig. 12e). In this sample the dominant grain size fraction is the very coarse-grained sand with 40.1% of total sample volume. Coarse and medium-grained sand classes compose 36.23% and 16.39% of total sample volume, respectively. Minor amounts of fine-grained sand (3.81%) and fine gravel (2.27%) are also documented. Eventually, tiny fractions of very fine-grained sand and silt-size material compose the fine tail of the curve with 0.84% and 0.35% of volume density, respectively (Fig. 12e).

Summarizing the main results obtained from thin section analysis, we observe a progressive broadening and coarsening of granulometric curves with different distribution of particles from LIM1 to ACQ1 samples (Fig. 13a). In coarse-grained samples (PES1 and ACQ1) the coarse, right tail of the distribution curves shows oscillating volume density values due to the presence of a few tens of grains providing higher data scattering. The comparison of

https://doi.org/10.5194/egusphere-2023-2636
Preprint. Discussion started: 15 November 2023

cumulative frequency distribution confirms the diminishing of the slope due to lowering sorting degree (Fig. 13b).

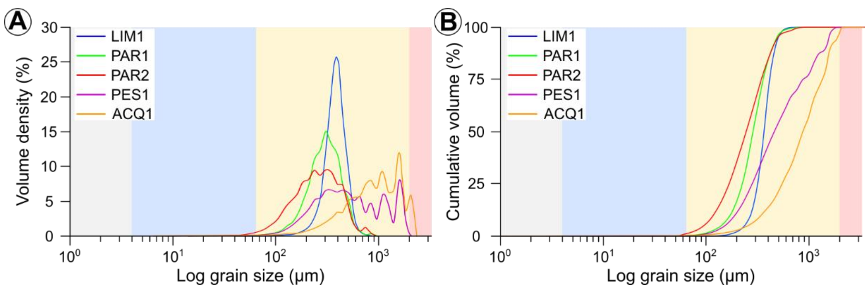

Figure 13. Comparison of grain size distributions obtained from image analysis technique applied to thin sections. (**a**) Volume density grain size distributions. (**b**) Cumulative volume percentage grain size distributions.

5.4 Laser granulometry vs. thin section grain size distributions

The comparison between volume density distribution curves acquired via optical granulometry and thin section analysis, shows striking similarities (Fig. 14). For all the 5 considered samples both methods provide similar overall shape of grain size distributions with almost overlapping modal peak values. Slight differences in modal peak height can be documented especially for highly to moderately sorted samples (LIM1 and PAR1), in which the grain size distribution curve obtained through image analysis has higher modal values compared to the laser granulometer data (Fig. 14a and b). On the same samples, laser granulometer technique recorded higher particle volumes in the right (coarse) tail of granulometric curve with respect to image analysis data. Tiny differences can be seen in the left (fine) tail of curves, with LIM1 displaying minor particle volume recorded by laser granulometry with respect to thin sections, while the opposite occurs for PAR1 sample. For the other 3 coarser and less sorted samples (PAR2, PES1 and ACQ1) the match between

https://doi.org/10.5194/egusphere-2023-2636
Preprint. Discussion started: 15 November 2023

the granulometric curves gained with different methods is good and the intercepts with X axis are almost coincident (Fig. 14c-e).

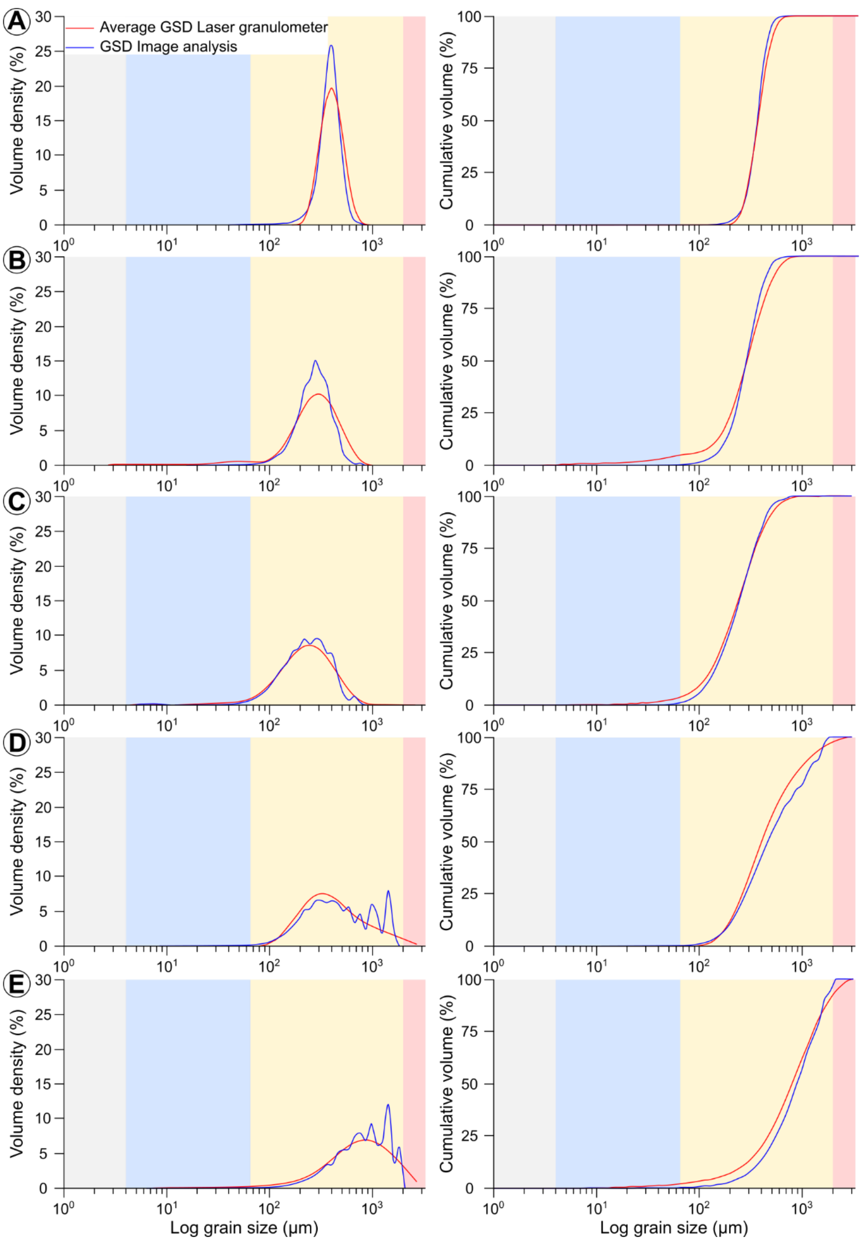

Figure 14. Comparison between grain size distributions extracted from laser granulometry and from image analysis. (**a**) LIM1 beach sample. (**b**) PAR1 fluvial sample. (**c**) PAR2 fluvial sample. (**d**) PES1 fluvial sample. (**e**) ACQ1 fluvial-deltaic sample. GSD, grain size distribution. GSD, grain size distribution.

https://doi.org/10.5194/egusphere-2023-2636
Preprint. Discussion started: 15 November 2023

The main differences are related to the right (coarse) tail of the curves, especially for PES1 and ACQ1 samples, where the thin section distribution curve displays volume density variability in the coarser grain size range. This data variability is induced by few very coarse (1-2 mm size) particles, which influence the final volume density distribution (Fig. 14d and e).

5.5 Volume-weighted mean diameter calculation

Calculations of volume-weighted mean diameter were performed with the formula reported in equation 2. The entire grain size datasets associated with thin sections of granular samples were considered. The foreshore beach sand sample LIM1, returns a value of volume-weighted mean diameter equal to 364.16 µm, while for the fluvial sand bar samples (PAR1 and PAR2) mean values of 296.54 µm and 256.08 µm are obtained, respectively. PES1 fluvial coarse sand shows a volume-weighted mean diameter of 625.83 µm, and the fossil deltaic sand ACQ1 sample provides a value of 955.79 µm. All the obtained mean diameter values are lower than the equivalent obtained through optical laser granulometry. We then applied a surface area correction factor (λ), as indicated in equation 3, to consider the deviations of grain shape from spherical particles (Fig. 15) (Davies et al., 2019; Johnson et al., 2021). λ factor was calculated for every sample and implemented in equation 2 as indicated in the modified volume-weighted mean diameter formula reported in equation 4. For LIM1 sample, the aspect ratio of grains spans from 1.01 to 7.01, with a mean value of 1.65 ± 0.49, thus equation 3 can be simplified and returns an average λ value of 1.17 ± 0.08 (Fig. 15a). By multiplying the volume-weighted mean diameter by λ factor, we obtain a corrected grain diameter of 425.35 µm. PAR1 has grain aspect ratio falling between 1.01

https://doi.org/10.5194/egusphere-2023-2636
Preprint. Discussion started: 15 November 2023

and 12.84, with a mean value of 1.89 ± 0.72, thus providing a mean λ correction factor of 1.19 ± 0.11 (Fig. 15b).

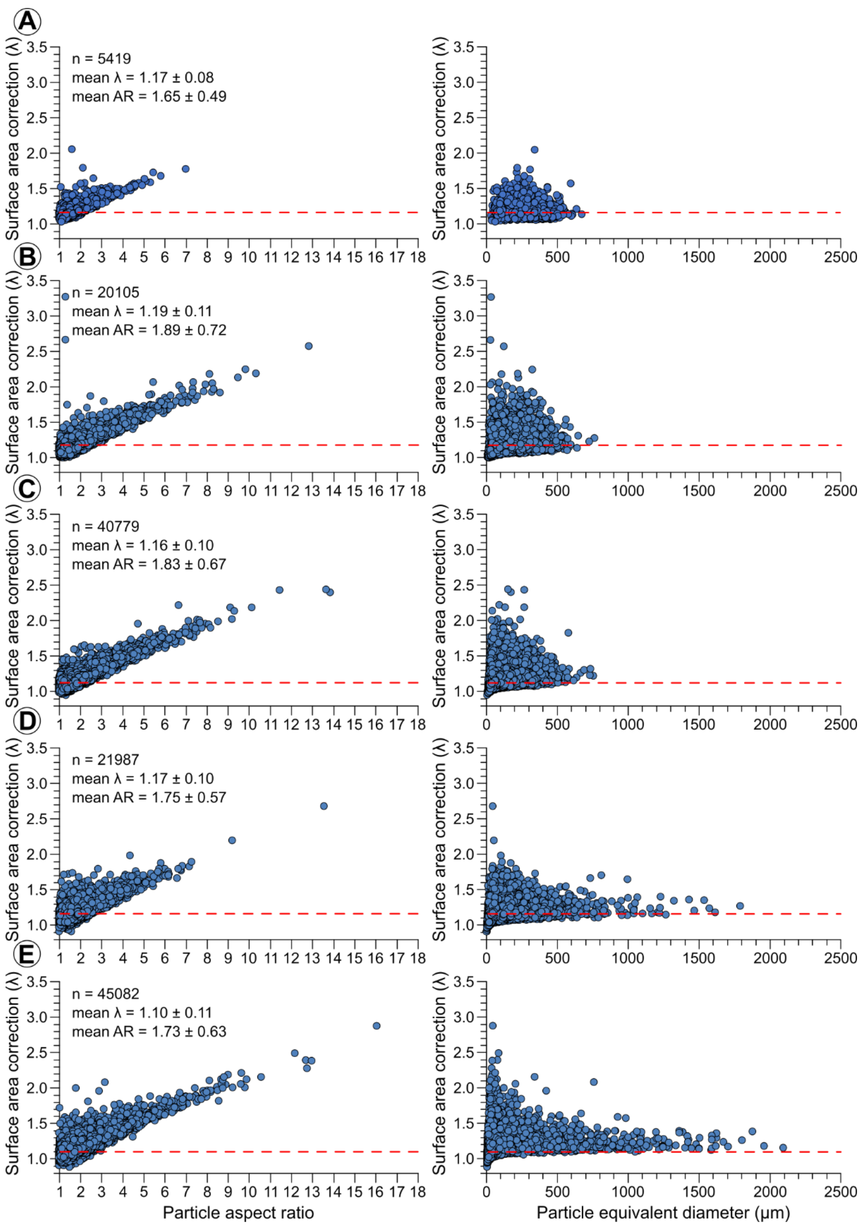

Figure 15. Graphs reporting the particle aspect ratio-surface area correction factor and particle equivalent diameter-surface area correction factor relationships for the analyzed sand samples. (**a**) LIM1 beach sample. (**b**) PAR1 fluvial sample. (**c**) PAR2 fluvial sample. (**d**) PES1 fluvial sample. (**e**) ACQ1 fluvial-deltaic sample.

https://doi.org/10.5194/egusphere-2023-2636
Preprint. Discussion started: 15 November 2023

The horizontal dashed red line indicates the average surface area correction factor. n, number of particles; λ, surface area correction factor; AR, particle aspect ratio.

The resulting corrected volume-weighted mean diameter is equal to 351.78 µm. For PAR2 sample, grains have aspect ratio comprised from 1.0 to 13.88 with an average value of 1.83 ± 0.67, giving a mean λ value of 1.16 ± 0.1 (Fig. 15c). The volume-weighted mean diameter corrected according to particle shape results 307.39 µm. PES1 is composed of grains with aspect ratio spanning from 1.0 to 13.55, with an average value of 1.75 ± 0.57, returning a mean λ correction factor of 1.17 ± 0.1 (Fig. 15d). Applying the correction to equation 4, the final volume-weighted mean diameter is equal to 731.08 µm. Eventually, ACQ1 sample is characterized by grains with aspect ratio between 1.0 and 16.06 with an average value of 1.73 ± 0.63, giving back a λ mean surface area correction factor of 1.10 ± 0.11 (Fig. 15e). The obtained corrected equivalent diameter for this sample is 1,055.64 µm. Volume-weighted mean diameter displays values close to the ones obtained through optical granulometry. The only exception is PES1 sample, which has an average grain size measured with laser granulometry 90-100 µm finer than the values calculated via image analysis on thin section.

6. Discussion

6.1 Comparison between 2D (image analysis) and 3D (laser granulometry) grain size analyses

Grain size distribution curves of analyzed samples obtained from 2D (image analysis) and 3D (laser granulometry) methods show striking similarities. The overall shape, skew (asymmetry) and modal peak position is equal in both the adopted methodologies (Fig. 14).

https://doi.org/10.5194/egusphere-2023-2636
Preprint. Discussion started: 15 November 2023

Slight differences can be traced in modal peak height, with data obtained through laser granulometry displaying typically lower modal height with respect to grain size distributions provided by image analysis from thin sections. Moreover, grain size distributions gained with the optical granulometer appear to be smoother especially on the coarser tail compared to image analysis data (Fig. 14). This can be explained by the usage of the 100 instrumental grain size classes adopted by the laser granulometer, which were extended also to image analysis grain size distributions. Such detailed subdivision of the 10 nm to 3,500 µm size interval in tiny frequency bins, caused variations in the coarser end of grain size distributions gained from image analysis. These variations are mainly related to the presence of a few tens of grains in coarser grain size classes inducing volume frequency oscillations. We employed the very same grain size classes for both analytical methods to allow precise comparison of data distribution, without the bias induced by different bin sizes. It is likely that the adoption of the standard sedimentological grain size classes (Udden-Wentworth scale) (Udden, 1914; Wentworth, 1922) could have provided more stable volume frequency results at the cost of less detail between different classes. Still, we preferred to prioritize and put emphasis on evidencing small differences between grain size classes rather than achieving volume frequency stability across the whole grain size distributions.

The comparison of volume-weighted mean diameters extracted from granulometry data, and the corrected volume-weighted mean diameters from image analysis technique provided matching results for 4 out of 5 total sand samples. In particular, for LIM1 sample, laser granulometry returned a mean equivalent diameter of 434 µm, while image analysis technique gave 425.3 µm. Fluvial sand PAR1 showed an equivalent diameter from laser granulometry of 352 µm, with related volume-weighted mean diameter of 351.8 µm, while for PAR2 returned diameter values of 304 and 307.4 µm, respectively. In the case of PES1, the laser granulometer measured a mean particle diameter of 639 µm, while data acquired

https://doi.org/10.5194/egusphere-2023-2636
Preprint. Discussion started: 15 November 2023

with image analysis provided a mean value of 731.1 µm. Eventually, for ACQ1 deltaic sand sample, laboratory grain size analysis gave a mean diameter of 1,050 µm, while image analysis technique provided a value of 1,055.6 µm. The only deviation from good and matching results was related to PES1 sample, which showed image analysis derived data 90-100 µm coarser than the equivalent diameter measured via laser granulometry. We explain this difference considering the mineralogical composition of the sample and the limits imposed by the involved analytical techniques. Apart from quartz, feldspar, and plagioclase, PES1 sample is composed of coarse aggregates of silt-clay matrix binding fine-grained siliciclastic grains (Fig. 16a). During manual tracing of particle outer boundaries, we treated these aggregates as single particles, without distinguishing the fine-grained particles interspersed within the matrix (Fig. 16b and c).

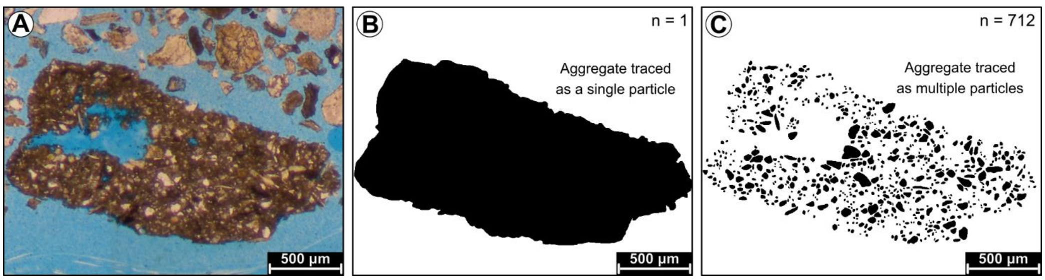

Figure 16. Soft aggregates issue encountered in manual digitization of PES1 sample. (**a**) Soft, ~2 mm-size, aggregate composed of clayish matrix embedding fine-grained siliciclastic particles. (**b**) Digitization strategy adopted in the present study for such clay aggregates. (**c**) Digitization of every particle composing the interior of the aggregate. n, number of traced grains.

Thin sectioning of loose granular media, proved to be a conservative method in preserving the original size and shape of weak sand framework components, minimizing the overall sample alteration. Conversely, laser granulometry operated via pressured air dispersion may cause alteration of original grain size in sensitive and mechanically weak samples (Storti and Balsamo, 2010; Cortinovis et al., 2019). Before the analyses we performed tests to set the instrumental parameters to be used granting the least sample alteration

(Supplementary material 1). In the case of PES1, which is the weakest sample, even the adoption of the most conservative analytical parameters was not enough to completely avoid sample damaging. This sample is the only one displaying aggregates whose matrix is made of clay minerals, which could have been damaged during laser granulometry analysis. In PES1 some alteration, related to splitting and partial disaggregation of soft silt-clay aggregates caused the fine-ward shift of the average particle diameter. In such weak sample types, we considered data derived from image analysis technique to be more reliable and representative of the real grain size distribution than laser granulometry analysis. The same alteration was not documented in the other 4 samples likely due to their different mineral composition and higher relative particle resistance, preventing any significant mechanical alteration of the original grain size during the analysis.

6.2 Volume-weighted mean diameter (D_w) vs. literature calculation methods

Mean particle diameter values based on optical granulometry and image analysis (corrected volume-weighted mean diameter) methods were compared with previously published and widely used calculation equations reported in the Appendix 1 (tables 2 and 3). In particular, we focused on the comparison with the method of moments (both arithmetic and geometric equation) (Krumbein and Pettijohn, 1938), the graphical method (geometric mean) (Folk and Ward, 1957), median, mode, arithmetic mean and area-weighted mean diameter. In comparing different equations, we assumed the mean diameter values extracted from the laser granulometer as reference, with relative differences between calculation formulas expressed as percentages (positive values represent grain diameter underestimation, while negative ones indicate overestimation with respect to the reference) (tables 2 and 3). Considering laser granulometry reference data, the arithmetic mean calculated with the method of moments, provides close results with the ones gained with the mean diameter formula employed by the optical granulometer (equation 5) (maximum difference in the average grain diameter of 0.36% from the reference value). Conversely, the geometrical mean of method of moments returns small percentage errors for well sorted samples (3.1% difference for LIM1 sample) with a progressively increasing error following sorting diminishing (from 16.4 to 24.4% error in PAR1, PAR2, PES1 and ACQ1 samples) (table 2).

Table 2: Comparison of results from different calculation equations applied to laser granulometry analyses

	Method of moments		Graphical method	GSD laser granulometry			
Sample name	Arithmetic (µm)	Geometric (µm)	Geometric (µm)	Sorting	D_m (µm)	Median (µm)	Mode (µm)
LIM1	434.7	420.5	420.6	0.37	434	420	419
PAR1	352.9	294.3	319.8	0.845	352	328	350
PAR2	305.1	252.7	261.1	0.877	304	267	286
PES1	640.3	492.6	487.5	1.029	639	455	386
ACQ1	1053.6	794.1	850.7	1.137	1050	897	1020
Sample name	Complementary percentage ratio with respect to volume-weighted mean diameter from laser granulometry (%)						
LIM1	-0.16	3.11	3.09	-	0	3.22	3.45
PAR1	-0.25	16.39	9.15	-	0	6.82	0.57
PAR2	-0.36	16.87	14.11	-	0	12.17	5.92
PES1	-0.20	22.91	23.71	-	0	28.79	39.59
ACQ1	-0.34	24.37	18.98	-	0	14.57	2.86

Table 2. Comparison of results given by different calculation formulas for grain size distribution acquired through laser granulometry. Calculation equations are reported in the Appendix 1. GSD, grain size distribution; D_m, average grain diameter (laser granulometer).

The same increasing error trend can be seen for the geometric mean of graphical method, with a maximum deviation of 23.7% calculated for PES1 sample. Eventually, the median of distribution curves is close to the mean diameter gained from laser granulometry only in the case of well sorted samples (deviation of 3.2 and 6.8% in LIM1 and PAR1, respectively), while it deviates far from it in more poorly sorted ones (PAR2, PES1 and ACQ1, with errors up to 28.8%). The mode can approximate the average diameter only in the case of weakly skewed grain size distributions (errors comprised from 0.5 to 5.9% in LIM1, PAR1, PAR2 and ACQ1), but it fails in the case of strongly skewed ones (39.6% deviation in PES1) (table 2).

https://doi.org/10.5194/egusphere-2023-2636
Preprint. Discussion started: 15 November 2023

Utilizing grain size distribution datasets extracted via image analysis technique (the corrected volume-weighted mean diameter is used as reference) the best results are provided by applying the arithmetic method of moments, with standard errors spanning from 1.7 to 3.9% in all samples. As already observed for laser granulometer size distributions, geometrical mean calculated with the method of moments returns good results only for well sorted samples, while tends to underestimate the mean diameter up to 25.3% of reference value in poorly sorted sands (Fig. 17 and table 3).

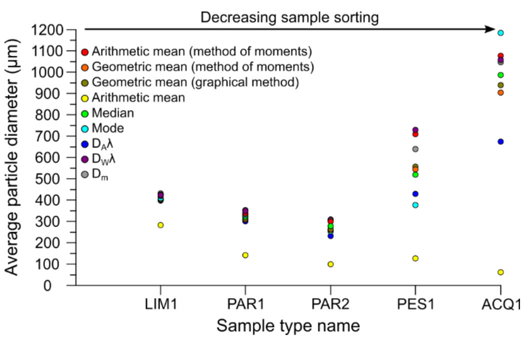

Figure 17. Comparison of average particle diameter values calculated with literature equations and the proposed volume-weighted mean diameter formula for the 5 considered sand samples. Used datasets are derived from thin sections analyzed with image analysis. $D_A\lambda$, area-weighted mean diameter (shape corrected); $D_W\lambda$, volume-weighted mean diameter (shape corrected). D_m, laser granulometer mean diameter.

Similar results are extracted from the geometric mean diameter formula of the graphical method, with the best result achieved for LIM1 sample (4.2% mean diameter underestimation) and worst attained for PES1 sand sample (23.7% diameter underestimation). Adoption of the median value grants good results for properly sorted samples (-0.4 to 7.7% in LIM1 and PAR1), while deviations become bigger in poorly sorted ones (10.9 and 28.9% in PAR2 and PES1, respectively) (Fig. 17). The mode follows similar trends and fails in describing weakly to poorly sorted granular media (errors from -12.2 to 48.6% in PAR2, PES1 and ACQ1). Severe mean diameter underestimation is documented

https://doi.org/10.5194/egusphere-2023-2636
Preprint. Discussion started: 15 November 2023

in the case of simple arithmetic mean diameter and area-weighted mean diameter with standard errors reaching 94.1 and 41.3%, respectively (Fig. 17 and table 3).

Table 3: Comparison of results from different calculation equations applied to image analysis grain size data

	Method of moments		Graphical method		GSD Image analysis				
Sample name	Arithmetic (µm)	Geometric (µm)	Geometric (µm)	Sorting	Arithmetic (µm)	Median (µm)	Mode (µm)	D_A λ (µm)	D_W λ (µm)
LIM1	415.4	403.2	407.5	0.329	283.8	427	411.2	401.4	425.3
PAR1	337.8	313.5	317.7	0.544	141.4	324.5	331	300	351.8
PAR2	302	264.6	267.2	0.757	98.63	273.9	256	232.7	307.4
PES1	709.6	546.3	557.4	1.097	127.8	519.6	376	428.9	731.1
ACQ1	1079.1	906.5	940.5	0.901	62.4	989.1	1185	674.6	1055.6
Sample name	Complementary percentage ratio with respect to volume-weighted mean diameter from image analysis (%)								
LIM1	2.33	5.19	4.18	-	33.27	-0.4	3.31	5.62	0
PAR1	3.98	10.88	9.69	-	59.81	7.76	5.91	14.72	0
PAR2	1.75	13.92	13.08	-	67.91	10.89	16.72	24.30	0
PES1	2.94	25.27	23.76	-	82.52	28.93	48.57	41.33	0
ACQ1	-2.22	14.12	10.90	-	94.09	6.29	-12.26	36.09	0

Table 3. Comparison of results provided by different calculation formulas for grain size distributions gained with image analysis. Calculation equations are reported in the Appendix 1. GSD, grain size distribution; D_Aλ, area-weighted mean diameter (shape corrected); D_Wλ, volume-weighted mean diameter (shape corrected).

Summarizing the comparative results, the proposed corrected volume-weighted mean diameter equation proves to be a reliable calculation formula and provides matching results with the arithmetic method of moments, as well as with data gained from laser granulometry technique. Conversely, the geometrical mean diameter of both method of moments and graphical method can describe only well to moderately sorted samples, while it struggles in poorly sorted ones. The same deviations, with even bigger magnitudes, can be highlighted by the adoption of the median and modal value as parameters describing grain size distributions. Similarly, the simple arithmetic mean, and area-weighted mean diameter are not reliable calculation equations, and their usage should be avoided as they show the highest difference from the reference (tables 2 and 3).

6.3 Shape correction factor (λ) vs. literature empirical correction parameters

https://doi.org/10.5194/egusphere-2023-2636
Preprint. Discussion started: 15 November 2023

In the past years, a lot of efforts were made to achieve robust conversion factors that could grant reliable 3D average particle diameter starting from 2D equivalent diameter distributions obtained with different analytical methods. Correction equations have been developed in different research areas of Earth Sciences spanning from sedimentology, planetary geology, to structural geology. Correction coefficients are based on geometrical considerations (Roethlisberger, 1955; Hughes, 1978b), statistical-mathematical relationships (Krumbein, 1935; Chayes, 1950; Greenman, 1951; Sahu, 1966; Rose, 1968; Johnson, 1994; Kong et al., 2005), empirical rules (Friedman, 1962a) or software aided simulations (Panozzo Heilbronner, 1992; Heilbronner and Bruhn, 1998). All these methods bring different correction coefficients to account for mean diameter underestimation related to random particle sectioning. Correction values are comprised between 1.0 and 1.5 and must by multiplied by the average grain diameter obtained from image analysis performed on rock thin sections (table 4). We tested the precision of equations proposed in literature by applying the correction coefficient to the volume-weighted mean diameter values obtained from the 5 studied sand samples. In this process, we did not multiply the mean diameter by the λ shape correction factor, thus using only the raw, uncorrected volume-weighted mean diameter values (table 4). Such a procedure allowed a direct comparison of λ shape correction factor with other correction parameters. By using our grain size datasets, closest results compared to the ones obtained with equation 4, are gained employing the correction factors proposed by Friedman (1958, 1962b), Sahu (1966), and Johnson (1994). Other correction methods (Krumbein, 1935; Chayes, 1950; Greenman, 1951; Hughes, 1978b; Panozzo, 1982; Panozzo Heilbronner, 1992; Kong et al., 2005) typically tend to overestimate the average grain diameter by a significant margin (table 4). This is especially true in the case of poorly sorted, coarse-grained samples (PES1 and ACQ1), while differences are less pronounced in well to moderately sorted and medium-grained ones (LIM1 and PAR1) (table 4). Although some of the correction methods discussed above provide close results with the

https://doi.org/10.5194/egusphere-2023-2636
Preprint. Discussion started: 15 November 2023

shape corrected volume-weighted mean diameter values, we prefer to apply different λ correction factors to different samples. This sample specific procedure should grant more reliable results, due to shape correction bound to the grain size distribution and particle form of each sample.

Table 4: Comparison of correction parameters with the presented original data

	Mean diameter of analyzed samples (µm)					
Literature correction method	LIM1	PAR1	PAR2	PES1	ACQ1	Correction factor
Krumbein (1935), Chayes (1950), Kong et al. (2005)	463.65	447.88	337.5	796.81	1216.91	1.2732
Krumbein (1935)	477.27	388.64	335.62	820.21	1252.65	1.3106
Greenman (1951)	494.86	402.39	348.03	851.04	1299.63	1.3589
Friedman (1958), (1962)	430.18	350.30	363.12	739.29	1129.07	1.1813
Sahu (1966)	412.15	335.62	289.83	708.31	1081.76	1.1318
Hughes (1978)	445.98	363.17	313.62	766.45	1170.55	1.2247
Panozzo (1982)	466.12	379.57	327.78	801.06	1223.41	1.28
Heilbronner (1992)	546.24	444.81	384.12	938.74	1433.68	1.5
Johnson (1994)	418.79	340.56	294.53	720.26	1099.92	1.15
D_w λ image analysis	425.35	351.78	307.39	731.08	1055.64	1.10-1.19
D_w uncorrected image analysis	364.16	296.54	256.08	625.83	955.79	
D_m laser granulometry	434	352	304	639	1050	

Table 4. Comparison of different published correction factors to be applied in switching from 2D to 3D grain size distributions. D_m, mean grain diameter (laser granulometer); D_w, volume-weighted mean diameter; λ, shape correction factor.

6.4 Representative number of particles-sorting relationship

In all the analyzed samples, we acquired large particle size datasets (> 5,000 particles), as we were interested in testing the reliability and reproducibility of mean diameter calculated with the proposed volume-weighted mean diameter formula. The number of digitized particles was higher in samples characterized by low sorting degree, and this was required to extract stable mean diameter values. At the same time, the adoption of large datasets allowed to check the critical number of particles required to achieve a certain standard error

https://doi.org/10.5194/egusphere-2023-2636
Preprint. Discussion started: 15 November 2023

associated with the mean diameter, using as reference the volume-weighted mean diameter calculated with all available particles.

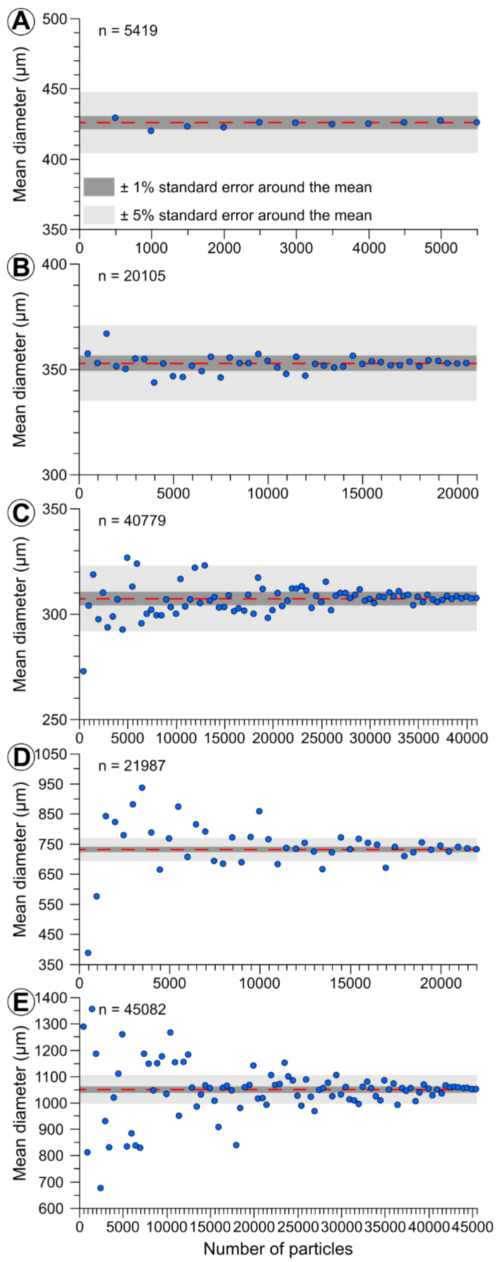

Figure 18. Volume-weighted mean diameter vs number of particles relationship calculated for 500 grains incremental bins. Standard error (±1 and 5%) intervals are calculated with respect to the average diameter

https://doi.org/10.5194/egusphere-2023-2636
Preprint. Discussion started: 15 November 2023

obtained from the entire grain size datasets (red dashed line). (**a**) LIM1 beach sample. (**b**) PAR1 fluvial sample. (**c**) PAR2 fluvial sample. (**d**) PES1 fluvial sample. (**e**) ACQ1 fluvial-deltaic sample. n, number of particles.

To do so, we calculated the volume-weighted mean diameter at incremental steps of 500 particles and we checked the deviation with respect to the reference value. At every calculation step, particles were randomized using a modified shuffle Matlab® algorithm to avoid any bias in particle extraction. We assumed two different confidence levels compiled at ± 1% and ± 5% standard error of the average diameter obtained with all available particles (Fig. 18). For LIM1 beach sand sample, volume-weighted mean diameter lays just outside the ± 1% standard error interval, using only 500-1,000 particles, while it becomes more stable and between ± 1% standard error for datasets > 1,500 grains (Fig. 18a). For this sample the minimum particle number is low due to the good sorting degree. PAR1 fluvial sand sample displays average diameter values always between the ± 5% error interval (already for 500 grains), but only using 12,500 particles or more, the calculated values fall in the ± 1% standard error (Fig. 18b). PAR2 sample shows a more marked scattering of data for limited particle number (< 5,000 grains), while the critical ± 5% error threshold is attained at 6,500 grains and the more restrictive ± 1% standard error is achieved for 29,500 particles (Fig. 18c). Mean diameter values for PES1 sample are characterized by strong variations up to 5,000-7,000 used grains, while they become more stable above 10,000 particles, reaching the ± 5% standard error threshold at 17,500 particle and the ± 1% error at 21,500 grains, respectively (Fig. 18d). Eventually, the poorly sorted ACQ1 sample displays volume-weighted mean diameter values outside the ± 5% error interval up to 10,000-15,000 grains. At least 27,500 particles are needed to calculate average diameter values in the ± 5% standard error interval and 42,500 grains must be used to achieve the ± 1% threshold (Fig. 18e). A decrease of sorting degree (widening of granulometric curves) from 0.37 to 1.137 causes an increase in the minimum number of particles to be used in average diameter calculation from 500 to 27,500 to reach the ± 5% standard error threshold (Fig. 19). To attain

https://doi.org/10.5194/egusphere-2023-2636
Preprint. Discussion started: 15 November 2023

the ± 1% error interval on the same samples, 1,500 to 42,500 particles are required (Fig. 19). We tested the importance of the number of particles used in sample with relatively simple size distribution curves (single mode and gentle curve asymmetry).

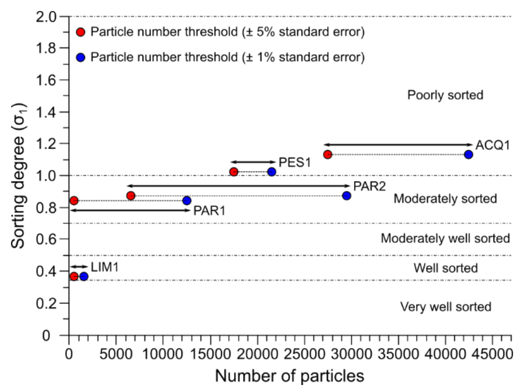

Figure 19. Critical particle number vs sorting degree relationship calculated for the 5 analyzed samples based on volume-weighted mean diameter calculations.

It is likely that samples with poorer sorting, multi-mode distributions and stronger asymmetry could require even larger particle amounts (Friedman, 1962a; Heilbronner and Barrett, 2014; Lopez-Sanchez, 2020). This aspect should be carefully considered when extracting average particle diameter from small datasets and results should be treated cautiously, being aware of the low reliability induced by limited data.

6.5 Fields of application and usefulness of the proposed method

Volume-weighted mean diameter proved to be a reliable parameter to describe 3D grain size distribution from 2D grain size datasets acquired through image analysis applied on thin sections. The addition of sample-specific λ shape correction factors facilitates the conversion from 2D to 3D grain size distributions. Moreover, the calculation formula is straightforward and can be easily used, without requiring specific stereological-

https://doi.org/10.5194/egusphere-2023-2636
Preprint. Discussion started: 15 November 2023

mathematical knowledge (Elias, 1967; Underwood, 1970; Russ, 1986; Gallagher et al., 2023). Our tests have been performed on loose sand samples, but the volume-weighted mean diameter could be particularly useful in the case of cohesive and hardened granular media not suitable to be analyzed through other laboratory techniques (optical granulometry, electro-resistivity methods, pipette, or sedimentation). Grain size analysis on such sample types must be conducted by means of microscopy characterization in conjunction with image analysis technique (Krumbein, 1935). Basic image analysis software, such as ImageJ, provides every required factor to be inserted in the calculation equation (Schneider et al., 2012). We preferred to manually digitize all the 2D grain size datasets employed to set the mean diameter formula, to achieve the maximum precision in defining particle shape and outer boundaries. However, as this procedure is extremely time consuming (7-10 days of work for each thin section image), it may be seen as poorly viable and suitable in the case numerous samples to be analyzed (Heilbronner and Barrett, 2014). In the past years, many efforts have been made to process large number of images both with semi-automatic and automatic methods (Mazzullo and Kennedy, 1985; Eicken, 1993; Heilbronner and Bruhn, 1998; Ketcham, 2005; Mock and Jerram, 2005; Gualda, 2006; Berger et al., 2011; Lopez-Sanchez and Llana-Fúnez, 2016). Image segmentation has become a more reliable, efficient and easy procedure, leading to the acquisition of thousands of grain size data in few hours of processing with acceptable errors (Heilbronner and Barrett, 2014). In recent years, some authors developed image segmentation algorithms which employ computer artificial intelligence and machine learning processes in particle segmentation, further reducing data acquisition time (Saxena et al., 2021). By taking advantage of these recent techniques, users should not be concerned about the minimum number of representative particles to be used in calculating volume-weighted mean diameter, even at the highest desired precision intervals. Following this, we encourage scientists of different research areas, to experiment and test the usefulness of the proposed corrected volume-weighted

https://doi.org/10.5194/egusphere-2023-2636
Preprint. Discussion started: 15 November 2023

mean diameter as it provided precise and reliable results in samples with different textural characteristics, grain size distributions and mineral compositions.

7. Concluding remarks

The correct measuring of particle size distributions and particle-grain mean diameters is fundamental in the study and characterization of both natural and artificial granular media. Several analytical procedures and calculation equations have been set up in the last decades. However, the comparison between 2D and 3D datasets acquired with different techniques is not straightforward. To help addressing this issue, we proposed the use of volume-weighted mean diameter, an easy-to-use equation designed to define 3D equivalent particle diameter from 2D datasets gained through image analysis technique. The corrected volume-weighted mean diameter equation that has been set is capable of accurately describing grain size distribution on different sample types. Apart for the volume-weighing, the equation takes also into account particle shapes and is suitable for granular samples with different textural characteristics and mineral compositions. The following conclusive points can be drawn from our study:

1- Volume-weighted mean diameter provides matching results with particle size data gained through optical granulometry technique, and combined with thin sectioning, can be useful in the case of weak or sensitive samples that can be partially compromised by laser diffraction or other analytical methodologies. In such sample types, 2D image analysis grants much more conservative and representative results than laser granulometry.
2- Employing both laser granulometry and image analysis datasets, volume-weighted mean diameter returns close results compared to the methods of moments

https://doi.org/10.5194/egusphere-2023-2636
Preprint. Discussion started: 15 November 2023

(arithmetic mean) equation. Conversely, other calculation formulas (geometric mean of method of moments, geometric mean of graphical method, median, and mode) proved to be less reliable and more sample sensitive (goodness of results may vary according to sample sorting and skewness).

3- The calculation of accurate and precise average diameter values requires an increasing particle number following the diminishing of sorting degree (widening of grain size distribution). However, automatic to semi-automatic particle identification and image analysis processing could help in reducing the time required for the acquisition of such large particle datasets.

4- The adoption of volume-weighted mean diameter provides reliable data and allows the estimation of 3D average diameter from 2D particle datasets. This process is based on a relatively simple equation, employing basic input parameters, without recurring to advanced stereology concepts or difficult mathematical equations.

Given the summary points described above, we suggest researchers working on different disciplines dealing with particle size determination to test the volume-weighted mean diameter equation and check whether it could be a viable solution for straightforward mean diameter calculation from 2D data distributions.

Declaration of competing interests

The authors declare that they have no known competing financial interests or personal relationships that could have appeared to influence the work reported in this paper.

Author contributions

https://doi.org/10.5194/egusphere-2023-2636
Preprint. Discussion started: 15 November 2023

Mattia Pizzati: Conceptualization, Supervision, Data curation, Formal analysis, Methodology, Writing original draft, Writing - review & editing, Validation.

Luciana Mantovani: Conceptualization, Data curation, Formal analysis, Methodology, Writing - review & editing.

Antonio Lisotti: Conceptualization, Data curation, Methodology.

Fabrizio Storti: Conceptualization, Supervision, Writing - review & editing.

Fabrizio Balsamo: Conceptualization, Supervision, Writing - review & editing, Validation, Funding acquisition.

Acknowledgements

This work has benefited from the equipment and framework of the COMP-HUB and COMP-R Initiatives, funded by the 'Departments of Excellence' program of the Italian Ministry for University and Research (MIUR, 2018-2022 and MUR, 2023-2027). This work was supported by the research project '*Earthquake cycle in shallow sediments'* (FIL Quota Incentivante, Bando competitivo di Ateneo per la Ricerca 2020, Azione 1) granted to Fabrizio Balsamo, funded by University of Parma and Cariparma. Andrea Comelli (University of Parma) is kindly acknowledged for thin section preparation.

Supplementary material

Details regarding the standard operating procedures adopted in optical granulometry analyses, XRD patterns, and high-resolution thin section photomosaics shown in Fig. 11 are reported in the online Supplementary material.

https://doi.org/10.5194/egusphere-2023-2636
Preprint. Discussion started: 15 November 2023

Appendix 1

Hereafter are listed and explained the equations of the calculation formulas used in comparing particle diameter values in tables 2 and 3. We adopted the equations implemented in GRADISTAT, grain size statistical analysis software (Blott and Pye, 2001). Arithmetic and geometric means from the method of moments have been used (Krumbein and Pettijohn, 1938), and the first one is defined as:

$$\bar{x}_a = \frac{\sum_{i=0}^{i=n} f m_m}{100} \qquad \text{(A1)}$$

where, $\bar{x}_a$ is the arithmetic mean, fm_m stands for the frequency percentage of particles at the midpoint (*m*) of each size class (*i*).

Conversely, the geometric mean of the method of moments is given by the equation:

$$\bar{x}_g = \frac{\sum_{i=0}^{i=n} f \ln m_m}{100} \qquad \text{(A2)}$$

where, $\bar{x}_g$ is the geometric mean, $f\ln m_m$ is the logarithmic frequency of particles at the midpoint (*m*) of each size class (*i*).

The graphical method has been employed as well, with the geometrical mean and sorting degree (Folk and Ward, 1957; Folk, 1974). The geometrical mean diameter is described by the equation:

$$M_G = \exp\frac{\ln P_{16} + \ln P_{50} + \ln P_{84}}{3} \qquad \text{(A3)}$$

where, M_G is the geometrical mean and P_{16}, P_{50} and P_{84} are the particle diameter values in metric units at the 16, 50 and 84% cumulative percentile of the particle size distribution curve, respectively.

https://doi.org/10.5194/egusphere-2023-2636
Preprint. Discussion started: 15 November 2023

Sorting degree (σ_1) is provided by the standard deviation associated with the logarithmic mean (Folk, 1974) and is given by the equation:

$$\sigma_1 = \frac{\Phi_{84} - \Phi_{16}}{4} + \frac{\Phi_{95} - \Phi_5}{6.6} \quad \text{(A4)}$$

in which, Φ is the grain diameter in phi units, at 5, 16, 84 and 95% cumulative percentile values of the particle size distribution curve, respectively.

References

Adams, J.: Sieve size statistics from grain measurement, J. Geol., 85, 209–227, 1977.

Agrawal, Y. C., McCave, I. N., and Riley, J. B.: Laser diffraction size analysis, in: Syvitski, J.M.P. (eds.) Principles, methods and application of particle size analysis., Cambridge University Press, Cambridge, UK., 119–128, 1991.

Bah, A. R., Kravchuk, O., and Kirchhof, G.: Fitting Performance of Particle-size Distribution Models on Data Derived by Conventional and Laser Diffraction Techniques, Soil Sci. Soc. Am. J., 73, 1101–1107, https://doi.org/10.2136/sssaj2007.0433, 2009.

Balsamo, F. and Storti, F.: Size dependent comminution, tectonic mixing and sealing behavior of a “structurally oversimplified” fault zone in poorly lithified sands: Evidence for a coseismic rupture?, Bull. Geol. Soc. Am., 123, 651–668, https://doi.org/10.1130/B30099.1, 2011.

Balsamo, F., Storti, F., Salvini, F., Silva, A. T., and Lima, C. C.: Structural and petrophysical evolution of extensional fault zones in low-porosity, poorly lithified sandstones of the Barreiras Formation, NE Brazil, J. Struct. Geol., 32, 1806–1826, https://doi.org/10.1016/j.jsg.2009.10.010, 2010.

Balsamo, F., Storti, F., and Gröcke, D.: Fault-related fluid flow history in shallow marine sediments from carbonate concretions, Crotone basin, south Italy, J. Geol. Soc. London, 169, 613–626, https://doi.org/10.1144/0016-76492011-109.Fault-related, 2012.

Barrett, P. J.: The shape of rock particles, a critical review, Sedimentology, 27, 291–303, 1980.

Basumallick, S.: A note on thin section mechanical analysis, J. Sediment. Res., 34, 194–195, https://doi.org/10.1306/74d7100f-2b21-11d7-8648000102c1865d, 1964.

Bense, V. F., Gleeson, T., Loveless, S. E., Bour, O., and Scibek, J.: Fault zone hydrogeology, Earth-Science Rev., 127, 171–192, https://doi.org/10.1016/j.earscirev.2013.09.008, 2013.

van den Berg, E. H., Bense, V. F., and Schlager, W.: Assessing textural variation in laminated sands using digital image analysis of thin sections, J. Sediment. Res., 73, 133–

https://doi.org/10.5194/egusphere-2023-2636
Preprint. Discussion started: 15 November 2023

143, https://doi.org/10.1306/061502730133, 2003.

Berger, A., Herwegh, M., Schwarz, J. O., and Putlitz, B.: Quantitative analysis of crystal/grain sizes and their distributions in 2D and 3D, J. Struct. Geol., 33, 1751–1763, https://doi.org/10.1016/j.jsg.2011.07.002, 2011.

Beuselinck, L., Govers, G., Poesen, J., Degraer, G., and Froyen, L.: Grain-size analysis by laser diffractometry: comparison with the sieve-pipette method, Catena, 32, 193–208, https://doi.org/10.1016/S0341-8162(98)00051-4, 1998.

Bianchi, G. G., Hall, I. R., McCave, I. N., and Joseph, L.: Measurement of the sortable silt current speed proxy using the Sedigraph 5100 and Coulter Multisizer IIe: Precision and accuracy, Sedimentology, 46, 1001–1014, https://doi.org/10.1046/j.1365-3091.1999.00256.x, 1999.

Billi, A.: Grain size distribution and thickness of breccia and gouge zones from thin (<1 m) strike-slip fault cores in limestone, J. Struct. Geol., 27, 1823–1837, https://doi.org/10.1016/j.jsg.2005.05.013, 2005.

Bittelli, M., Andrenelli, M. C., Simonetti, G., Pellegrini, S., Artioli, G., Piccoli, I., and Morari, F.: Shall we abandon sedimentation methods for particle size analysis in soils?, Soil Tillage Res., 185, 36–46, https://doi.org/10.1016/j.still.2018.08.018, 2019.

Blenkinsop, T. G.: Cataclasis and Processes of Particle Size Reduction, Pageoph, 136, 59–86, 1991.

Blott, S. J. and Pye, K.: Gradistat: A grain size distribution and statistics package for the analysis of unconsolidated sediments, Earth Surf. Process. Landforms, 26, 1237–1248, https://doi.org/10.1002/esp.261, 2001.

Blott, S. J. and Pye, K.: Particle size distribution analysis of sand-sized particles by laser diffraction: An experimental investigation of instrument sensitivity and the effects of particle shape, Sedimentology, 53, 671–685, https://doi.org/10.1111/j.1365-3091.2006.00786.x, 2006.

Blott, S. J., Croft, D. J., Pye, K., Saye, S. E., and Wilson, H. E.: Particle size analysis by laser diffraction, Geol. Soc. Spec. Publ., 232, 63–73, https://doi.org/10.1144/GSL.SP.2004.232.01.08, 2004.

de Boer, G. B. J., de Weerd, C., Thoenes, D., and Goossens, H. W. J.: Laser diffraction spectrometry: Fraunhofer diffraction versus Mie scattering, Part. Charact., 4, 14–19, 1987.

Boggs, S.: Petrology of sedimentary rocks, Cambridge University Press, New York, 600 pp., 2009.

Bowman, E. T., Soga, K., and Drummond, W.: Particle shape characterisation using Fourier descriptor analysis, Geotechnique, 51, 545–554, https://doi.org/10.1680/geot.2001.51.6.545, 2001.

Bridges, N. T. and Muhs, D. R.: Duststones on mars: Source, transport, deposition, and erosion, SEPM Spec. Publ., 102, 169–182, https://doi.org/10.2110/pec.12.102.0169, 2012.

Van Den Bril, K. and Swennen, R.: Sedimentological control on carbonate cementation in the Luxembourg Sandstone Formation, Geol. Belgica, 12, 3–23, 2009.

https://doi.org/10.5194/egusphere-2023-2636
Preprint. Discussion started: 15 November 2023

Brooks, H. L., Steel, E., and Moore, M.: Grain-Size Analysis of Ancient Deep-Marine Sediments Using Laser Diffraction, Front. Earth Sci., 10, 1–24, https://doi.org/10.3389/feart.2022.820866, 2022.

Bryon, D. N., Atherton, M. P., and Hunter, R. H.: The interpretation of granitic textures from serial thin sectioning, image analysis and three-dimensional reconstruction, Mineral. Mag., 59, 203–211, https://doi.org/10.1180/minmag.1995.059.395.05, 1995.

Bull, W. B.: Relation of Textural (CM) Patterns to Depositional Environment of Alluvial-fan Deposits, J. Sediment. Petrol., Vol. 32, 211–216, https://doi.org/10.1306/74d70c7c-2b21-11d7-8648000102c1865d, 1962.

Buller, A. T. and McManus, J.: Modes of turbidites deposition deduced from grain-size analyses, Geol. Mag., 109, 491–500, 1973.

Burger, H. and Skala, W.: Comparison of sieve and thin-section technique by a Monte-Carlo model, Comput. Geosci., 2, 123–139, 1976.

Bush, J.: Derivation of a Size-Frequency Curve from the Cumulative Curve, J. Sediment. Petrol., Vol. 21, 178–182, https://doi.org/10.1306/d4269463-2b26-11d7-8648000102c1865d, 1951.

Cadigan, R. A.: Geologic interpretation of grain-size distribution measurements of Colorado Plateau sedimentary rocks, J. Geol., 69, 121–143, 1961.

Cavazza, W., Braga, R., Reinhardt, E. G., and Zanotti, C.: Influence of host-rock texture on the morphology of carbonate concretions in a meteoric diagenetic environment, J. Sediment. Res., 79, 377–388, https://doi.org/10.2110/jsr.2009.047, 2009.

Celia Magno, M., Venti, F., Bergamin, L., Gaglianone, G., Pierfranceschi, G., and Romano, E.: A comparison between Laser Granulometer and Sedigraph in grain size analysis of marine sediments, Meas. J. Int. Meas. Confed., 128, 231–236, https://doi.org/10.1016/j.measurement.2018.06.055, 2018.

Chayes, F.: A simple point counter for thin-section analysis, Am. Mineral., 34, 1–11, 1949.

Chayes, F.: On the bias of grain-size measurements made in thin section, J. Geol., 58, 156–160, 1950.

Cheetham, M. D., Keene, A. F., Bush, R. T., Sullivan, L. A., and Erskine, W. D.: A comparison of grain-size analysis methods for sand-dominated fluvial sediments, Sedimentology, 55, 1905–1913, https://doi.org/10.1111/j.1365-3091.2008.00972.x, 2008.

Coakley, J. P. and Syvitski, J. P. M.: SediGraph technique, in: Syvitski, J.M.P. (eds.) Principles, methods and application of particle size analysis., Cambridge University Press, Cambridge, UK., 129–142, 1991.

Cooper, M. R. and Hunter, R. H.: Precision serial lapping, imaging and three-dimensional reconstruction of minus-cement and post-cementation intergranular pore-systems in the Penrith Sandstone of north-western England, Mineral. Mag., 59, 213–220, https://doi.org/10.1180/minmag.1995.059.395.06, 1995.

Cortinovis, S., Balsamo, F., and Storti, F.: Influence of analytical operating procedures on particle size distributions in carbonate cataclastic rocks, J. Struct. Geol., 128, 103884, https://doi.org/10.1016/j.jsg.2019.103884, 2019.

https://doi.org/10.5194/egusphere-2023-2636
Preprint. Discussion started: 15 November 2023

Cruz-Orive, L. M.: Distribution-free estimation of sphere size distributions from slabs showing overprojection and truncation, with a review of previous methods, J. Microsc., 131, 265–290, 1983.

Dapples, E. C., Krumbein, W. C., and Sloss, L. L.: Petrographic and lithologic attributes of sandstones, J. Geol., 61, 291–317, 1953.

Davies, T. R. H., McSaveney, M. J., and Reznichenko, N. V.: What happens to fracture energy in brittle fracture? Revisiting the Griffith assumption, Solid Earth, 10, 1385–1395, https://doi.org/10.5194/se-10-1385-2019, 2019.

Davis, S. N. and DeWiest, R. J. M.: Hydrogeology, Wiley & Sons, New York, 463 pp., 1966.

Dimmen, V., Rotevatn, A., and Nixon, C. W.: The Relationship between Fluid Flow, Structures, and Depositional Architecture in Sedimentary Rocks: An Example-Based Overview, Geofluids, 1–19, https://doi.org/10.1155/2020/3506743, 2020.

Doan, M.-L. and Gary, G.: Rock pulverization at high strain rate near the San Andreas fault, Nat. Geosci., 2, 709–712, 2009.

Dodd, R. T.: Accretion of the ordinary chondrites, Earth Planet. Sci. Lett., 30, 281–291, 1976.

Dutton, S. P., White, C. D., Willis, B. J., and Novakovic, D.: Calcite cement distribution and its effect on fluid flow in deltaic sandstone, Frontier Formation, Wyoming, Am. Assoc. Pet. Geol. Bull., 86, 2007–2021, 2002.

Easterbrook, D. J.: Principles of Geomorphology, McGraw-Hill, New York, 462 pp., 1969.

Eicken, H.: Automated image analysis of ice thin sections: instrumentation, methods and extraction of stereological textural parameters, J. Glaciol., 39, 341–352, 1993.

Eisenhour, D. D.: Determining chondrule size distributions from thin-section measurements, Meteorit. Planet. Sci., 31, 243–248, https://doi.org/10.1111/j.1945-5100.1996.tb02019.x, 1996.

Elias, H.: Stereology, Springer-Verlag, New York, 335 pp., 1967.

Engelder, J.-T.: Cataclasis and the generation of fault gouge, Geol. Soc. Am. Bull., 85, 1515–1522, https://doi.org/10.1130/0016-7606(1974)85<1515:catgof>2.0.co;2, 1974.

Eychenne, J. and Engwell, S. L.: The grainsize of volcanic fall deposits: Spatial trends and physical controls, GSA Bull., 135, 1844–1858, https://doi.org/10.1130/b36275.1, 2022.

Faure, G. and Mensing, T. M.: Introduction to Planetary Science: The geological perspective, Springer, Dordrecht, The Netherlands, 1–526 pp., https://doi.org/10.1007/978-1-4020-5544-7, 2007.

Fernlund, J. M. R.: 3-D image analysis size and shape method applied to the evaluation of the Los Angeles test, Eng. Geol., 77, 57–67, https://doi.org/10.1016/j.enggeo.2004.08.002, 2005.

Fetter, C. W.: Applied Hydrogeology, 3rd ed., Prentice-Hall, Englewood Cliffs, New Jersey, USA, 691 pp., 1994.

https://doi.org/10.5194/egusphere-2023-2636
Preprint. Discussion started: 15 November 2023

Folk, R. L.: A review of grain-size parameters, Sedimentology, 6, 73–93, 1966.

Folk, R. L.: Petrology of sedimentary rocks, 170 pp., https://doi.org/10.1017/CBO9781107415324.004, 1974.

Folk, R. L. and Ward, W. C.: Brazos River bar: a study in the significance of grain size parameters, J. Sediment. Petrol., 27, 3–26, 1957.

Francus, P.: Using image analysis to estimate quantitatively some microstructural parameters of detrital sediments, Geol. Belgica, 2–3, 173–180, 1999.

Fraser, H. J.: Experimental study of the porosity and permeability of clastic sediments, J. Geol., 43, 910–1010, 1935.

Freeman, B. and Ferguson, C. C.: Deformation mechanism maps and micromechanics of rocks with distributed grain sizes, J. Geophys. Res., 91, 3849–3860, 1986.

Friedman, G. M.: Determination of sieve-size distribution from thin-section data for sedimentary petrological studies, J. Geol., 66, 394–416, 1958.

Friedman, G. M.: Comparison of Moment Measures for Sieving and Thin-Section Data in Sedimentary Petrological Studies, SEPM J. Sediment. Res., Vol. 32, 15–25, https://doi.org/10.1306/74d70c36-2b21-11d7-8648000102c1865d, 1962a.

Friedman, G. M.: On sorting, sorting coefficients, and the lognormality of the grain size distribution of sandstones, J. Geol., 70, 737–753, 1962b.

Friedman, G. M.: In defence of point counting analysis: hypothetical experiments versus real rocks, Sedimentology, 4, 247–253, 1965.

Gallagher, C., Kerr, E., and McFadden, S.: Particle size distribution for additive manufacturing powder using stereological corrections, Powder Technol., 429, 118873, https://doi.org/10.1016/j.powtec.2023.118873, 2023.

Garzanti, E.: Petrographic classification of sand and sandstone, Earth-Science Rev., 192, 545–563, https://doi.org/10.1016/j.earscirev.2018.12.014, 2019.

Giachetti, T., Trafton, K. R., Wiejaczka, J., Gardner, J. E., Watkins, J. M., Shea, T., and Wright, H. M. N.: The products of primary magma fragmentation finally revealed by pumice agglomerates, Geology, 49, 1307–1311, https://doi.org/10.1130/G48902.1, 2021.

Goldbery, R. and Richardson, D.: The influence of bulk shape factors on settling velocities of natural sand-sized sedimentary suites, Sedimentology, 36, 125–136, 1989.

Grassy, R. G.: Use of the Microprojector in the Mechanical Analysis of Small Samples of River Sand, J. Sediment. Petrol., Vol. 13, 47–57, https://doi.org/10.1306/d4269193-2b26-11d7-8648000102c1865d, 1943.

Greenman, N. N.: The mechanical analysis of sediments from thin-section data, J. Geol., 59, 447–462, 1951.

Griffiths, J. C.: Grain-size distribution and reservoir-rock characteristics, Am. Assoc. Pet. Geol. Bull., 36, 205–229, https://doi.org/10.1126/science.58.1489.27.b, 1952.

Griffiths, J. C.: Measurement of the properties of sediments, J. Geol., 69, 487–497, 1961.

Grotzinger, J. P. and Milliken, R. E.: The sedimentary rock record of mars: Distribution, origins, and global stratigraphy, 1–48 pp., https://doi.org/10.2110/pec.12.102.0001, 2012.

Gualda, G. A. R.: Crystal size distributions derived from 3D datasets: Sample size versus uncertainties, J. Petrol., 47, 1245–1254, https://doi.org/10.1093/petrology/egl010, 2006.

Harrell, J. A. and Eriksson, K. A.: Empirical Conversion Equations for Thin-Section and Sieve Derived Size Distribution Parameters, J. Sediment. Petrol., Vol. 49, 273–280, https://doi.org/10.1306/212f7711-2b24-11d7-8648000102c1865d, 1979.

Heilbronner, R.: Automatic grain boundary detection and grain size analysis using polarization micrographs or orientation images, J. Struct. Geol., 22, 969–981, https://doi.org/10.1016/S0191-8141(00)00014-6, 2000.

Heilbronner, R. and Barrett, S.: Image Analysis in Earth Sciences - Microstructures and Textures of Earth Materials, Springer, Heidelberg, 520 pp., 2014.

Heilbronner, R. and Bruhn, D.: The influence of three-dimensional grain size distributions on the rheology of polyphase rocks, J. Struct. Geol., 20, 695–705, 1998.

Heilbronner, R. and Keulen, N.: Grain size and grain shape analysis of fault rocks, Tectonophysics, 427, 199–216, https://doi.org/10.1016/j.tecto.2006.05.020, 2006.

Higgins, M. D.: Numerical modeling of crystal shapes in thin sections: Estimation of crystal habit and true size, Am. Mineral., 79, 113–119, 1994.

Higgins, M. D.: Measurement of crystal size distributions, Am. Mineral., 85, 1105–1116, https://doi.org/10.2138/am-2000-8-901, 2000.

Hirsch, D. M.: Controls on porphyroblast size along a regional metamorphic field gradient, Contrib. to Mineral. Petrol., 155, 401–415, https://doi.org/10.1007/s00410-007-0248-y, 2008.

Hughes, D. W.: A disaggregation and thin section analysis of the size and mass distribution of the chondrules in the Bjurbole and Chainpur meteorites, Earth Planet. Sci. Lett., 38, 391–400, 1978a.

Hughes, D. W.: Chondrule mass distribution and the Rosin and Weibull statistical functions, Earth Planet. Sci. Lett., 39, 371–376, 1978b.

Jébrak, M.: Hydrothermal breccias in vein-type ore deposits: A review of mechanisms, morphology and size distribution, Ore Geol. Rev., 12, 111–134, https://doi.org/10.1016/S0169-1368(97)00009-7, 1997.

Jerram, D. A. and Higgins, M. D.: 3D analysis of rock textures: Quantifying igneous microstructures, Elements, 3, 239–245, https://doi.org/10.2113/gselements.3.4.239, 2007.

Jerram, D. A., Mock, A., Davis, G. R., Field, M., and Brown, R. J.: 3D crystal size distributions: A case study on quantifying olivine populations in kimberlites, Lithos, 112, 223–235, https://doi.org/10.1016/j.lithos.2009.05.042, 2009.

Johnson, M. R.: Thin section grain size analysis revisted, Sedimentology, 41, 985–999, 1994.

Johnson, S. E., Song, W. J., Vel, S. S., Song, B. R., and Gerbi, C. C.: Energy Partitioning,

https://doi.org/10.5194/egusphere-2023-2636
Preprint. Discussion started: 15 November 2023

Dynamic Fragmentation, and Off-Fault Damage in the Earthquake Source Volume, J. Geophys. Res. Solid Earth, 126, 1–38, https://doi.org/10.1029/2021JB022616, 2021.

Kaminski, E. and Jaupart, C.: The size distribution of pyroclasts and the fragmentation sequence in explosive volcanic eruptions, J. Geophys. Res. Solid Earth, 103, 29759–29779, https://doi.org/10.1029/98jb02795, 1998.

Keller, W. D.: Size distribution of sand in some dunes, beaches, and sandstones, Am. Assoc. Pet. Geol. Bull., 29, 215–221, 1945.

Kellerhals, R., Shaw, J., and Arora, V. K.: On grain size from thin sections, J. Geol., 83, 79–96, 1975.

Kennedy, S. K. and Mazzullo, J.: Image analysis method of grain size measurement, in: Syvitski, J.M.P. (eds.) Principles, methods and application of particle size analysis., Cambridge University Press, Cambridge, UK., 76–87, 1991.

Ketcham, R. A.: Computational methods for quantitative analysis of three-dimensional features in geological specimens, Geosphere, 1, 32–41, https://doi.org/10.1130/GES00001.1, 2005.

Keulen, N., Heilbronner, R., Stünitz, H., Boullier, A. M., and Ito, H.: Grain size distributions of fault rocks: A comparison between experimentally and naturally deformed granitoids, J. Struct. Geol., 29, 1282–1300, https://doi.org/10.1016/j.jsg.2007.04.003, 2007.

Kimura, S., Ito, T., and Minagawa, H.: Grain-size analysis of fine and coarse non-plastic grains: comparison of different analysis methods, Granul. Matter, 20, 1–15, https://doi.org/10.1007/s10035-018-0820-3, 2018.

Konert, M. and Vandenberghe, J.: Comparison of laser grain size analysis with pipette and sieve analysis: A solution for the underestimation of the clay fraction, Sedimentology, 44, 523–535, https://doi.org/10.1046/j.1365-3091.1997.d01-38.x, 1997.

Kong, M., Bhattacharya, R. N., James, C., and Basu, A.: A statistical approach to estimate the 3D size distribution of spheres from 2D size distributions, Bull. Geol. Soc. Am., 117, 244–249, https://doi.org/10.1130/B25000.1, 2005.

Kranck, K.: Grain-size characteristics of turbidites, Geol. Soc. Spec. Publ., 15, 83–92, https://doi.org/10.1144/GSL.SP.1984.015.01.05, 1984.

Krumbein, W. C.: The mechanical analysis of fine-grained sediments, J. Sediment. Petrol., 2, 140–149, 1932.

Krumbein, W. C.: Thin-section mechanical analysis of indurated sediments, J. Geol., 43, 482–496, 1935.

Krumbein, W. C.: Size Frequency Distributions of Sediments and the Normal Phi Curve, SEPM J. Sediment. Res., Vol. 8, 84–90, https://doi.org/10.1306/d4269008-2b26-11d7-8648000102c1865d, 1938.

Krumbein, W. C.: Measurement and geological significance of shape and roundness of sedimentary particles, J. Sediment. Petrol., 11, 64–72, 1941a.

Krumbein, W. C.: The Effects of Abrasion on the Size, Shape and Roundness of Rock Fragments, J. Geol., 49, 482–520, https://doi.org/10.1086/624985, 1941b.

https://doi.org/10.5194/egusphere-2023-2636
Preprint. Discussion started: 15 November 2023

Krumbein, W. C. and Pettijohn, F. J.: Manual of Sedimentary Petrography, Appleton Century Crofts, New York, 549 pp., 1938.

Krumbein, W. C. and Sloss, L.: Stratigraphy and Sedimentation, W.H. Freeman and Co, San Francisco, 660 pp., 1963.

Kwan, A. K. H., Mora, C. F., and Chan, H. C.: Particle shape analysis of coarse aggregate using digital image processing, Cem. Concr. Res., 29, 1403–1410, https://doi.org/10.1016/S0008-8846(99)00105-2, 1999.

Liu, Y., Liu, X., and Sun, Y.: QGrain: An open-source and easy-to-use software for the comprehensive analysis of grain size distributions, Sediment. Geol., 423, 105980, https://doi.org/10.1016/j.sedgeo.2021.105980, 2021.

Lopez-Sanchez, M. A.: Which average, how many grains, and how to estimate robust confidence intervals in unimodal grain size populations, J. Struct. Geol., 135, 104042, https://doi.org/10.1016/j.jsg.2020.104042, 2020.

Lopez-Sanchez, M. A. and Llana-Fúnez, S.: An extension of the Saltykov method to quantify 3D grain size distributions in mylonites, J. Struct. Geol., 93, 149–161, https://doi.org/10.1016/j.jsg.2016.10.008, 2016.

Luther, A., Axen, G., and Selverstone, J.: Particle-size distributions of low-angle normal fault breccias: Implications for slip mechanisms on weak faults, J. Struct. Geol., 55, 50–61, https://doi.org/10.1016/j.jsg.2013.07.009, 2013.

Maithel, S. A., Brand, L. R., and Whitmore, J. H.: A methodology for disaggregation and textural analysis of quartz-cemented sandstones, J. Sediment. Res., 89, 599–609, https://doi.org/10.2110/jsr.2019.35, 2019.

Marone, C. and Scholz, C. H.: Particle size distribution and microstructures within simulated fault gouge, J. Struct. Geol., 11, 799–814, 1989.

Martin, P. M. and Mills, A. A.: Size and shape of near-spherical Allegan chondrules, Earth Planet. Sci. Lett., 38, 385–390, 1978.

Matthews, M. D.: The effect of grain shape and density on size measurement, in: Syvitski, J.M.P. (eds.) Principles, methods and application of particle size analysis., Cambridge University Press, Cambridge, UK., 22–33, 1991a.

Matthews, M. D.: The effect of pretreatment on size analysis, in: Syvitski, J.M.P. (eds.) Principles, methods and application of particle size analysis., Cambridge University Press, Cambridge, UK., 34–42, 1991b.

Mazzullo, J. and Kennedy, S. K.: Automated measurement of the nominal sectional diameters of individual sedimentary particles, J. Sediment. Res., 55, 593–595, 1985.

McBride, E. F., Milliken, K. L., Cavazza, W., Cibin, U., Fontana, D., Picard, M. D., and Zuffa, G. G.: Heterogeneous distribution of calcite cement at the outcrop scale in Tertiary sandstones, northern Apennines, Italy, Am. Assoc. Pet. Geol. Bull., 79, 1044–1063, https://doi.org/10.1306/8d2b21c3-171e-11d7-8645000102c1865d, 1995.

McCave, I. N. and Syvitski, J. M. P.: Principles and methods of geological particle size analysis, in: Syvitski, J.M.P. (eds.) Principles, methods and application of particle size analysis., Cambridge University Press, Cambridge, UK., 3–21, 1991.

https://doi.org/10.5194/egusphere-2023-2636
Preprint. Discussion started: 15 November 2023

McCave, I. N., Bryant, R. J., Cook, H. F., and Coughanowr, C. A.: Evaluation of a laser-diffraction size analyzer for use with natural sediments, J. Sediment. Res., 56, 561–564, 1986.

McPhie, J., Doyle, M., and Allen, R.: Volcanic Tectures: a guide to the interpretation of textures in volcanic rocks, University of Tasmania, Hobart, Australia, 196 pp., 1993.

Means, W. D. and Park, Y.: New experimental approach to understanding igneous texture, Geology, 22, 323–326, https://doi.org/10.1130/0091-7613(1994)022<0323:NEATUI>2.3.CO;2, 1994.

Menzies, J.: Micromorphological analyses of microfabrics and microstructures indicative of deformation processes in glacial sediments, in: Maltman, A.J., Hubbard, B. & Hambrey, M.J. (eds.) Deformation of Glacial Materials. Geological Society of London, Special Publications, 176., 245–257, 2000.

Middleton, G. V.: Hydraulic interpretation of sand size distributions, J. Geodyn., 84, 405–426, 1976.

Milligan, T. G. and Kranck, K.: Electroresistance particle size analyzers, in: Syvitski, J.M.P. (eds.) Principles, methods and application of particle size analysis., Cambridge University Press, 8, 109–118, 1991.

Mock, A. and Jerram, D. A.: Crystal size distributions (CSD) in three dimensions: Insights from the 3D reconstruction of a highly porphyritic rhyolite, J. Petrol., 46, 1525–1541, https://doi.org/10.1093/petrology/egi024, 2005.

Molnia, B. L.: Glacial Marine Sedimentation, Plenum Press, New York, 844 pp., 1983.

Montheil, L., Toy, V. G., Scott, J. M., Mitchell, T. M., and Dobson, D. P.: Impact of Coseismic Frictional Melting on Particle Size, Shape Distribution and Chemistry of Experimentally-Generated Pseudotachylite, Front. Earth Sci., 8, 1–12, https://doi.org/10.3389/feart.2020.596116, 2020.

Mora, C. F. and Kwan, A. K. H.: Sphericity, shape factor, and convexity measurement of coarse aggregate for concrete using digital image processing, Cem. Concr. Res., 30, 351–358, https://doi.org/10.1016/S0008-8846(99)00259-8, 2000.

Morad, S., Ketzer, J. M., and DeRos, F.: Spatial and temporal distribution of diagenetic alterations in siliciclastic rocks: implication for mass transfer in sedimentary basins, Sedimentology, 47, 95–120, https://doi.org/10.1046/j.1365-3091.2000.00007.x, 2000.

Morgan, D. J. and Jerram, D. A.: On estimating crystal shape for crystal size distribution analysis, J. Volcanol. Geotherm. Res., 154, 1–7, https://doi.org/10.1016/j.jvolgeores.2005.09.016, 2006.

Moss, A. J.: The physical nature of common sandy and pebbly deposits. Part 1, Am. J. Sci., 260, 337–373, 1962.

Mozley, P. S. and Davis, J. M.: Relationship between oriented calcite concretions and permeability correlation structure in an alluvial aquifer, Sierra Ladrones Formation, New Mexico, J. Sediment. Res., 66, 11–16, https://doi.org/10.1306/D4268293-2B26-11D7-8648000102C1865D, 1996.

Mutti, E.: Turbidite sandstones, Agip, Istituto di Geologia, Università di Parma, San Donato

https://doi.org/10.5194/egusphere-2023-2636
Preprint. Discussion started: 15 November 2023

Milanese, Milan, 256 pp., 1992.

Nichols, G.: Sedimentology and Stratigraphy, Wiley, Chichester, UK, 419 pp., https://doi.org/10.1017/CBO9781107415324.004, 2009.

Packham, G. H.: Volume, weight and number-frequency analysis of sediments from thin-sections data, J. Geol., 63, 50–58, 1955.

Panozzo Heilbronner, R.: Two-dimensional analysis of shape-fabric using projections of digitized lines in a plane, Tectonophysics, 95, 279–294, 1983.

Panozzo Heilbronner, R.: The autocorrelation function: an image processing tool for fabric analysis, Tectonophysics, 212, 351–370, 1992.

Panozzo, R.: Determination of size distribution of spheres from size distributions of circular section by Monte Carlo methods, Microsc. Acta, 86, 37–48, 1982.

Passchier, C. W. and Trouw, R. A.: Microtectonics, 2nd ed., Springer, Berlin, 366 pp., 2005.

De Pater, I. and Lissauer, J. J.: Planetary Sciences, Cambridge University Press, Cambridge, UK., 528 pp., 2001.

Pettijohn, F. J., Potter, P. E., and Siever, R.: Sand and sandstone, Springer, New York, 618 pp., 1972.

Pickering, K. T. and Hiscott, R. N.: Deep Marine Systems: Processes, Deposits, Environments, Tectonics and Sedimentation, Wiley, 672 pp., 2015.

Pizzati, M., Balsamo, F., Storti, F., Mozafari, M., Iacumin, P., Tinterri, R., and Swennen, R.: From axial parallel to orthogonal groundwater flow during fold amplification: insights from carbonate concretion development during the growth of the Quattro Castella Anticline, Northern Apennines, Italy, J. Geol. Soc. London., 175, 806–819, 2018.

Van Der Plas, L.: Preliminary note on the granulometric analysis of sedimentary rocks, Sedimentology, 1, 145–157, 1962.

Powers, M. C.: A New Roundness Scale for Sedimentary Particles, J. Sediment. Petrol., Vol. 23, 117–119, https://doi.org/10.1306/d4269567-2b26-11d7-8648000102c1865d, 1953.

Ranalli, G.: Grain size distribution and flow stress in tectonites, J. Struct. Geol., 6, 443–447, 1984.

Roberson, S. and Weltje, G. J.: Inter-instrument comparison of particle-size analysers, Sedimentology, 61, 1157–1174, https://doi.org/10.1111/sed.12093, 2014.

Roethlisberger, H.: An adequate method of grain size determination in sections, J. Geol., 63, 579–584, 1955.

Rose, H. E.: The determination of the grain-size distribution of a spherical granular material embedded in a matrix, Sedimentology, 10, 293–309, 1968.

Rosenfeld, M. A., Jacobsen, L., and Ferm, J. C.: A comparison of sieve and thin-section technique for size analysis, J. Geol., 61, 114–132, 1953.

Russ, J. C.: Practical Stereology, Plenum Press, New York, 194 pp., 1986.

https://doi.org/10.5194/egusphere-2023-2636
Preprint. Discussion started: 15 November 2023

Russ, J. C.: Computer-assisted Microscopy: The Measurement and Analysis of Images, Plenum Press, New York, 453 pp., 1990.

Sahagian, D. L. and Proussevitch, A. A.: 3D particle size distributions from 2D observations: stereology for natural applications, J. Volcanol. Geotherm. Res., 84, 173–196, https://doi.org/10.1016/S0377-0273(98)00043-2, 1998.

Sahu, B. K.: Depositional Mechanisms from the Size Analysis of Clastic Sediments, J. Sediment. Res., 34, 73–83, https://doi.org/10.1306/74d70fce-2b21-11d7-8648000102c1865d, 1964.

Sahu, B. K.: Thin section analysis of sandstones on weight-frequency basis, Sedimentology, 7, 255–259, 1966.

Sammis, C. G. and Ben-Zion, Y.: Mechanics of grain-size reduction in fault zones, J. Geophys. Res. Solid Earth, 113, 1–12, https://doi.org/10.1029/2006JB004892, 2008.

Saxena, N., Day-Stirrat, R. J., Hows, A., and Hofmann, R.: Application of deep learning for semantic segmentation of sandstone thin sections, Comput. Geosci., 152, 104778, https://doi.org/10.1016/j.cageo.2021.104778, 2021.

Schäfer, A. and Teyssen, T.: Size, shape and orientation of grains in sands and sandstones: image analysis applied to rock thin sections, Sediment. Geol., 52, 251–271, 1987.

Schneider, C. A., Rasband, W. S., and Eliceiri, K. W.: NIH Image to ImageJ: 25 years of image analysis, Nat. Methods, 9, 671–675, 2012.

Schulte, P., Lehmkuhl, F., Steininger, F., Loibl, D., Lockot, G., Protze, J., Fischer, P., and Stauch, G.: Influence of HCl pretreatment and organo-mineral complexes on laser diffraction measurement of loess-paleosol-sequences, Catena, 137, 392–405, https://doi.org/10.1016/j.catena.2015.10.015, 2016.

Seelos, K. and Sirocko, F.: RADIUS - Rapid particle analysis of digital images by ultra-high-resolution scanning of thin sections, Sedimentology, 52, 669–681, https://doi.org/10.1111/j.1365-3091.2005.00715.x, 2005.

Selley, R. .: Applied Sedimentology, 1–523 pp., https://doi.org/10.1017/CBO9781107415324.004, 2001.

Sibson, R. H.: Fault rocks and fault mechanisms, J. Geol. Soc. London, 133, 191–213, 1977.

Singer, J. K., Anderson, J. B., Ledbetter, M. T., McCave, I. N., Jones, K. P. N., and Wright, R.: An assessment of analytical techniques for the size analysis of fine-grained sediments, J. Sediment. Petrol., 58, 534–543, https://doi.org/10.1306/212f8de6-2b24-11d7-8648000102c1865d, 1988.

Smith, R. E.: Grain size measurement in thin section and in grain mount, J. Sediment. Res., 36, 841–843, https://doi.org/10.1306/74d71979-2b21-11d7-8648000102c1865d, 1966.

Song, B. R., Johnson, S. E., Song, W. J., Gerbi, C. C., and Yates, M. G.: Coseismic damage runs deep in continental strike-slip faults, Earth Planet. Sci. Lett., 539, 116226, https://doi.org/10.1016/j.epsl.2020.116226, 2020.

https://doi.org/10.5194/egusphere-2023-2636
Preprint. Discussion started: 15 November 2023

Spencer, D. W.: The interpretation of grain size distribution curves of clastic sediments, J. Sediment. Petrol., 33, 180–190, 1952.

Sperazza, M., Moore, J. N., and Hendrix, M. S.: High-resolution particle size analysis of naturally occurring very fine-grained sediment through laser diffractometry, J. Sediment. Res., 74, 736–743, https://doi.org/10.1306/031104740736, 2004.

Stauffer, P. H.: Thin section size analysis: a further note, Sedimentology, 7, 261–263, 1966.

Stipp, M. and Tullis, J.: The recrystallized grain size piezometer for quartz, Geophys. Res. Lett., 30, 1–5, https://doi.org/10.1029/2003GL018444, 2003.

Storti, F. and Balsamo, F.: Particle size distributions by laser diffraction: sensitivity of granular matter strength to analytical operating procedures, Solid Earth, 1, 25–48, https://doi.org/10.5194/se-1-25-2010, 2010.

Storti, F., Billi, A., and Salvini, F.: Particle size distributions in natural carbonate fault rocks: Insights for non-self-similar cataclasis, Earth Planet. Sci. Lett., 206, 173–186, https://doi.org/10.1016/S0012-821X(02)01077-4, 2003.

Syvitski, J. P. M., LeBlanc, K. W. G., and Asprey, K. W.: Interlaboratory, interinstrument calibration experiment, in: Syvitski, J.M.P. (eds.) Principles, methods and application of particle size analysis., Cambridge University Press, Cambridge, UK., 174–193, 1991a.

Syvitski, J. P. M., Asprey, K. W., and Clattenburg, D. A.: Principles, design, and calibration of settling tubes, in: Syvitski, J.M.P. (eds.) Principles, methods and application of particle size analysis., Cambridge University Press, Cambridge, UK., 45–63, 1991b.

Tafesse, S., Fernlund, J. M. R., and Bergholm, F.: Digital sieving-Matlab based 3-D image analysis, Eng. Geol., 137–138, 74–84, https://doi.org/10.1016/j.enggeo.2012.04.001, 2012.

Taylor, M. A.: Quantitative measures for shape and size of particles, Powder Technol., 124, 94–100, https://doi.org/10.1016/S0032-5910(01)00476-4, 2002.

Théodon, L., Debayle, J., and Coufort-Saudejaud, C.: Morphological characterization of aggregates and agglomerates by image analysis: A systematic literature review, Powder Technol., 430, 119033, https://doi.org/10.1016/j.powtec.2023.119033, 2023.

Tiab, D. and Donaldson, E. C.: Petrophysics, 2nd ed., Elsevier, Burlington, USA, 889 pp., 2004.

Torabi, A. and Fossen, H.: Spatial variation of microstructure and petrophysical properties along deformation bands in reservoir sandstones, Am. Assoc. Pet. Geol. Bull., 93, 919–938, https://doi.org/10.1306/03270908161, 2009.

Udden, J. A.: Mechanical composition of clastic sediments, Geol. Soc. Am. Bull., 25, 655–744, https://doi.org/10.1130/gsab-25-655, 1914.

Underwood, E. E.: Quantitative Stereology, 2nd ed., Addison-Wesley Publishing Company, Reading, MA, USA, 274 pp., 1970.

Wadell, H.: Sphericity and roundness of rock particles, J. Geol., 41, 310–331, 1933.

https://doi.org/10.5194/egusphere-2023-2636
Preprint. Discussion started: 15 November 2023

Wadell, H.: Volume, shape and roundness of quartz particles, J. Geol., 43, 250–280, 1935.

Washburn, A. L.: Geocryology: A Survey of Periglacial Processes and Environment, Edward Arnold Ltd., London, 406 pp., 1979.

Weiner, B. B.: Particle sizing using photon correlation spectroscopy, in: Barth, H.G. (eds.) Modern methods of particle size analysis., Wiley, New York, 93–116, 1984.

Wentworth, C. K.: A Laboratory and Field Study of Cobble Abrasion, J. Geol., 27, 507–521, https://doi.org/10.1086/622676, 1919.

Wentworth, C. K.: A Scale of Grade and Class Terms for Clastic Sediments, J. Geol., 30, 377–392, https://doi.org/10.1086/622910, 1922.

Wicksell, S. D.: The corpuscle problem, a mathematical study of a biometric problem, Biometrika, 17, 84–99, 1925.

Zieg, M. J. and Marsh, B. D.: Crystal size distributions and scaling laws in the quantification of igneous textures, J. Petrol., 43, 85–101, https://doi.org/10.1093/petrology/43.1.85, 2002.